One-step preparation method for multiple drug-loaded lipid-based calcium carbonate nanoparticles

（複数の薬物を搭載した脂質・炭酸カルシウムナノ粒子を
一段階で調製する方法に関する研究）

2018

Peng Jian Qing

Contents

Preface

Nowadays, combination therapies have been widely used in the cancer treatments. A variety of combinations composed of small molecular drugs, genes and proteins were involved in clinical treatments and scientific researches. The application of combination therapies aims at increasing therapeutic effects, decreasing side effects and realizing reversion of multidrug resistance.

To achieve the synergistic effects in combination therapies, a number of functional drug delivery systems (DDSs) have been developed for the co-delivery of multiple drugs. DDSs for combination therapies require several characteristics, including simplified preparation process for encapsulation of drugs, co-delivery to diseased regions, stimuli-responsive release of cargos after cellular uptake, and sufficient stability of DDSs *in vivo*. However, most of the DDSs cannot be widely applied for both the small molecular drug combinations and macro-molecule/small-molecule drug combinations.

In the present studies, I developed a nanoplatform consisted of calcium carbonate ($CaCO_3$), lipids, polyelectrolytes and targeting moieties for co-delivery of drug/drug or protein/drug. For 'one-step' preparation of the nanoparticles, I used the ethanol injection method as the key factor. The encapsulation of multiple drugs is based on the electrostatic interactions and hydrophobic interactions. $CaCO_3$ in the nanoparticles played a role as a stimuli-responsive unit for pH-sensitive drug release. The inherent pH sensitivity of $CaCO_3$ would lead to decomposition of $CaCO_3$ under the acidic conditions such as the tumor microenvironment and endosomal environment. Released Ca^{2+} ions and high concentration of H^+ ions would further break the balance of electrostatic interactions among the components in the nanoparticles. The polyelectrolyte is an indispensable component in the nanoparticles. As polyanion, polyacrylic acids was used in the nanoparticle for the small molecular drug combination to increase the encapsulation of the hydrophilic drug and promote the pH-sensitive drug release. Here, proteins are a category of polyelectrolytes as well. The proteins can be encapsulated by the same

nanoplatform developed for the small drug combinations after optimization. Importantly, the nanoplatform that I designed here meets the requirements listed above for the combination therapies and has the potential of wide application for not only hydrophilic/hydrophobic small molecular drug combinations but also macro-molecule/small-molecule drug combinations.

Chapter I   One-step formation of lipid-polyacrylic acid-calcium carbonate nanoparticles for co-delivery of doxorubicin and curcumin

1. Introduction

In cancer treatments, combination therapies are widely applied in patients to achieve enhanced therapeutic efficacy and reduction of side-effects. As a superior strategy to circumvent multi-drug resistant (MDR) effects, combination therapies are generally applied for advanced tumor [1, 2] and terminal cancer patients [3]. A large number of drug delivery systems (DDSs) have been developed, with the aim of achieving targeted drug delivery to tumor tissues and cells. However, conventional single drug DDSs cannot easily be applied for combination therapies, especially for lipophilic and hydrophilic drug combinations.

Previous studies have indicated that the combination of doxorubicin (Dox) and curcumin (Cur) is a promising combination therapy for cancer treatment [2, 4]. Since the application of Dox is limited by cardiotoxicity and the emergence of the MDR effect. Cur, with a wide range of pharmacological effects, has been applied to overcome the MDR problem and ameliorate the side effects [4, 5]. A variety of nanocarriers has been developed in expectation of improving the solubility of Cur and realizing co-delivery of both Dox and Cur. Wang *et al.* developed Cur-Dox/MPEG-PCL micelles [6]. During their preparation, Cur and MPEG-PCL were first self-assembled into a core-shell-structured Cur/MPEG-PCL micelle, and then Dox was encapsulated in a buffer (pH 7.4). Barui *et al.* separately encapsulated Cur and Dox into ligand-modified liposomes using a film dispersion method and a pH gradient method, respectively [7]. In such DDSs, separated procedures are inevitable for encapsulation because of the diverse levels of water solubility of the drugs. This complexity in preparation restricts the potential application of such DDSs due to insufficient reproducibility, *in vivo* instability, asynchronous bio-distribution, and so on. Therefore, a nanoplatform exploiting a 'one-step' formation method for combination

therapies is in need.

Calcium carbonate ($CaCO_3$) has been widely studied as a carrier or component of nanoparticles in order to facilitate the delivery of drugs and genes [8, 9]. In the presence of polyanion such as DNA, $CaCO_3$ nanoparticles can be formed. The presence of Ca^{2+} and CO_3^{2-} ions that interacted with the DNA can form the DNA/$CaCO_3$ co-precipitation and enhance transfection efficiency [10]. Moreover, the inherent pH sensitivity of $CaCO_3$ might be useful to promote the dissociation of nanoparticles and endosome/lysosome escape under low pH conditions [11, 12]. Considering that the $CaCO_3$ was formed by the Ca^{2+} and CO_3^{2-} ions, it was capable to form the $CaCO_3$ simultaneously in the preparation of nanoparticles as a pH-sensitive inducer for drug release.

To increase the encapsulation efficiency of Dox, a water-soluble drug, a polyanion polyacrylic acid (PAA) was employed in the current study. Previous studies have shown that PAA and Dox can form complexes with a pH-dependent interaction [13]. Based on the results of a previous study, I chose a higher molecular weight PAA to achieve a high Dox encapsulation and a condensed structure for the PAA/Dox complexes. I designed a one-step formation method for a novel PEGylated lipid/PAA/$CaCO_3$ ternary system encapsulating Cur and Dox (LPCCD), aiming at increased tumor inhibitory effects and decreased cardiotoxicity [14]. After formulation optimization, the pH sensitivity, cellular uptake, *in vitro* tumor suppression, *in vivo* bio-distribution and safety of the LPCCD nanoparticles were studied.

2. Materials and methods

2.1 Materials and reagents

Egg lecithin (EPC), Cur and PAA (molecular weight: 25 kDa) were purchased from Wako Pure Chemical Industries (Osaka, Japan). *N*-(Carbonyl-methoxypolyethyleneglycol 2000)-1,2-distearoyl-sn-glycero-3-phosphoethanolamine (DSPE-PEG$_{2000}$) was obtained from NOF corporation (Tokyo, Japan). 1,2-dioleoyl-3-trimethylammonium-propane (DOTAP) was obtained from Avanti Polar Lipids

(Alabaster, AL, USA). Dox hydrochloride was provided by Tokyo Chemical Industry Co., Ltd. (Tokyo, Japan). The other inorganic chemicals were obtained from Nacalai Tesque (Kyoto, Japan). All organic solvents of analytical grade were purchased from Sigma-Aldrich (St. Louis, MO, USA). Water used in all experiments was prepared through Direct-Q UV (Merck Millipore, Merck KGaA, Darmstadt, Germany.).

2.2 Cells and animals

HepG2 human hepatoma cells were obtained from RIKEN (Tokyo, Japan). All cell culture media were purchased from Thermo Fisher Scientific (Waltham, MA USA).

Male ddY mice (25–27 g) and Wistar rats (230–280 g) supplied by Kyudo Co., Ltd. (Kumamoto, Japan) were fed with a standard laboratory diet and were housed at an ambient temperature and humidity in air-conditioned chambers before the experiments. All animal experiments were conducted in full compliance with the Guideline for Animal Experimentation at Nagasaki University.

2.3 Preparation and optimization of nanoparticles

The ethanol injection method was used in the preparation of this ternary system. A 1 M $CaCl_2$ ethanol solution, a 3 mg/mL Cur ethanol solution and a 10 mg/mL Dox water solution were prepared as stock solutions. A certain amount of EPC, DOTAP and DSPE-PEG was dissolved in 8 mL of ethanol. Under stirring, 0.2 mL of $CaCl_2$ solution, 1 mL of Cur solution and 0.5 mL of Dox solution were added dropwise to the lipid mixture solution in this sequence and stirred for another 1 h at room temperature (ethanol phase). Meanwhile, a 5 mM Na_2CO_3 water solution including 1.25% glucose was prepared. After a certain amount of PAA was solubilized in 40 mL of the Na_2CO_3/glucose solution and stirred for another 1 h (water phase, pH 6.8), the ethanol phase was added dropwise to the water phase with stirring for 2 h at room temperature. Then, the obtained mixture was maintained in a rotary evaporator (EYELA, Tokyo, Japan) under vacuum for 30 min at 40°C to evaporate the ethanol and concentrate the mixture to 10 mL. The obtained suspension was vortexed for 3 min and passed through a 0.8 μm filter to produce the LPCCD nanoparticles. In the preparation of a LPC blank carrier, the Cur and Dox

solutions were not added, and the procedure was identical in all other respects.

In the optimization of the formulation, the $CaCO_3$ concentration was varied and the ratio of PAA/DOTAP and DOTAP/EPC were studied. The diameter, polydispersity index (PDI), ζ potential and drug content of the nanoparticles were taken into consideration for the evaluation and confirmation of the optimized formulation.

2.4 Characterization of LPC and LPCCD

Particle size, PDI and ζ potential of the LPC and LPCCD were measured using a Zetasizer Nano ZS (Malvern, UK). To investigate size variation of the lipid nanoparticles under different pH conditions, 0.01 M pH 7.4 Hepes buffer or 0.01 M pH 5.5 Mes buffer were used for the dilution of the nanoparticles at a ratio of 3:1 (v/v). Changes in the size distribution of the LPC and LPCCD were recorded after a 2 h incubation.

Drug content, drug loading capacity (DL) and encapsulation efficiency (EE) of Dox and Cur were determined using high performance liquid chromatography (HPLC) with a UV detector (SPD-10A, Shimadzu, Kyoto, Japan). Briefly, 50 μL of the LPCCD solution was added to 5 mL of a 1% Triton X-100 solution. The solution was sonicated for 1 min and centrifuged at $12,000 \times g$ for 10 min (KUBOTA, Tokyo, Japan). The supernatant was analyzed using a mobile phase of 5% acetic acid: acetonitrile = 60:40 (v/v) at $\lambda = 420$ nm to determine the Cur concentration in the LPCCD. For the measurement of Dox concentration, a mobile phase of 0.3% sodium dodecyl sulphate (adjusting pH to 2.7 using phosphoric acid): acetonitrile: methanol = 60:40:1 (v/v) at $\lambda = 484$ nm was used. The mobile phase was delivered at 1 mL/min through a C_{18} column (Cosmosil-Paq, 4.6×150 mm, particle diameter 5 μm). DL and EE were calculated in accordance with the following equations:

$$DL\ (wt.\%) = \frac{Weight_{drug\ load}}{Weight_{nanopartilce}} \times 100 \qquad 1\text{-}1$$

$$EE\ (wt.\%) = \frac{Weight_{load}}{Weight_{feed}} \times 100 \qquad 1\text{-}2$$

2.5 pH-sensitive drug release

Drug release behavior was monitored using a membrane dialysis technique. 0.01 M

pH 7.4 Hepes buffer (including 0.1% Tween 80) and 0.01M pH 5.5 Mes buffer (including 0.1% Tween 80) were prepared to simulate the physiological environment and lysosome/endosome microenvironment, respectively. A LPCCD solution (0.2 mL) was placed into a dialysis bag (molecular weight cutoff: 12 kDa, Visking dialysis tube, Nihon Medical Science, Inc., Osaka, Japan) and exposed to 20 mL of pH 7.4 or pH 5.5 buffer. In addition, 0.2 mL of LPCCD solution with 10% fetal bovine serum (FBS; v/v) was also exposed to 20 mL of pH 7.4 buffer to determine the effect of serum on the stability of LPCCD. In a shaking water bath, the drug release was determined for 30 h at 37°C. At certain intervals, 0.1 mL of medium was withdrawn and the same amount of fresh medium was replenished. The concentration of Dox and Cur was determined using HPLC.

2.6 Hemolysis activity

Fresh rat arterial blood was centrifuged at $1,630 \times g$ for 10 min in pH 7.4 phosphate-buffered saline (PBS) to collect the red blood cells (RBCs). This step was repeated three times and the RBCs were resuspended in PBS. LPC or liposomes (prepared using the same amount of EPC, DOTAP and DSPE-PEG with the ethanol injection method) at various concentrations of lipids were incubated with a 10 % (v/v) RBC suspension at a ratio of 1:4 (v/v) and shaken in a water bath at 37°C for 1 h. Water and PBS were incubated with the RBC suspension using the same procedure, as a positive and negative control, respectively. After a 1 h incubation, the mixture was centrifuged at $1,630 \times g$ for 10 min and the supernatant was analyzed using a spectrophotometer (UV-1600, Shimadzu, Kyoto, Japan) at $\lambda = 550$ nm. The hemolysis percentage was calculated using the following equation:

$$\text{Hemolysis (\%)} = \frac{Absorbance_{sample} - Absorbance_{negative\ control}}{Absorbance_{positive\ control} - Absorbance_{negative\ control}} \times 100 \qquad \text{1-3}$$

2.7 In vitro cellular uptake

HepG2 cells were cultured in Dulbecco's modified Eagle's medium (DMEM) including 10% FBS and penicillin (100 U/mL)/streptomycin (100 µg/mL) at 37°C, 5% CO_2 and 90% relative humidity. For the cellular uptake evaluation, the cells were seeded

at a density of 1×10^5 cells/dish in 35 mm glass-base dishes. After a 12 h incubation, the cells were incubated with free Dox, Dox + Cur (1:1, mol/mol) and LPCCD (final concentration of 10 μM Dox) in FBS-free medium for a certain period of time at 37°C. Then, the supernatant was removed and the cells were washed using PBS (pH 7.4) three times. The cells were fixed in 4% paraformaldehyde for 15 min and washed using PBS again. After two drops of Slow Fade Diamond® (Thermo Fisher Scientific) were added, the samples were observed using confocal microscopy (Carl Zeiss Microimaging GmbH, Jena, Germany). To quantify the DOX cellular uptake, a fluorescence-activated cell-sorting flow cytometer (Beckman Coulter, Brea, CA, USA) was employed. The cells were seeded in 24-well plates at a density of 1×10^5 cells/well and pre-incubated for 24 h. Free Dox, Dox + Cur (1:1, mol/mol) and LPCCD (final concentration of 10 μM Dox) in FBS-free medium were added to each well, respectively. After incubation with the samples for 4 h, the supernatant was removed. The cells were washed with PBS and trypsinized in accordance with a standard protocol. After resuspension of the cells in 0.5 mL of PBS, fluorescence of the Dox was analyzed.

2.8 In vitro cytotoxicity

For an evaluation of cytotoxicity, the cells were seeded in 96-well plates at a density of 1×10^4 cells/well. Dox, Dox + Cur (1:1, mol/mol), LPC and LPCCD at various concentrations were added to the wells after a 12 h incubation. The cells were further incubated for 48 h, the medium was removed and the cells were washed with PBS. DMEM (100 μL) including 10 μL of cell counting kit-8 (Dojindo, Kumamoto, Japan) was added to each well and incubated for 1 h. The absorbance was measured at 450 nm using a microplate photometer (Multiskan™ FC, Thermo Fisher Scientific). Blank wells and untreated cells served as a negative control and positive control, respectively.

2.9 Bio-distribution of the nanoparticles

A free Dox + Cur solution and LPCCD (at an equivalent Dox concentration of 0.4 mg/mL and Cur concentration of 0.24 mg/mL) were intravenously injected in ddY mice at a Dox dose of 3 mg/kg. Mice were anesthetized using a drug mix (butorphanol,

medetomidine and midazolam) 3 h after the injection. Blood was taken from the inferior vena cava, and the heart, liver, spleen, lungs and kidneys were harvested and weighed. Dox and Cur were extracted as reported in a previous study [15]. Briefly, organs were homogenized using a mixed solution of isopropanol and 1 M HCl (1:1, v/v) and incubated at 4°C for 1 h. The homogenates were centrifuged at $1,630 \times g$ for 15 min, and the supernatants were centrifuged again at $15,000 \times g$ for 15 min. In the case of determining the drug concentration in plasma, the blood was centrifuged at $1,500 \times g$ for 10 min. The plasma supernatant was mixed with an isopropanol:1 M HCl = 1:1 (v/v) mixture and acetonitrile for the detection of Dox and Cur. The supernatants were analyzed using a fluorescence spectrometer (RF-5300PC, Shimadzu, Kyoto, Japan). For the detection of Dox, the excitation (Ex) and emission (Em) wavelength was 500 and 590 nm, respectively. An Ex/Em of 440/500 nm was used in the detection of Cur. Standard curves of Dox and Cur were prepared using blank organ extracts.

2.10 Histopathological analysis of cardiotoxicity

Free Dox and LPCCD were injected intravenously in ddY mice at a 5 mg/kg Dox equivalent once daily for 3 days. Six hours following the last injection, a histopathological analysis was performed on the heart. Briefly, after tissue perfusion, the heart was harvested and fixed using 4% paraformaldehyde, immersed in sucrose solution and embedded in O.C.T compound. The frozen tissues were sliced at a 5 μm thickness and stained using hematoxylin and eosin (H&E). A morphological evaluation was performed using a microscope (Carl Zeiss, Jena, Germany).

2.11 Statistical analysis

The data are presented as mean ± standard deviations (S.D.) of at least three independent experiments. Significant differences were identified using Student's t-test and one-way ANOVA analysis followed by Bonferroni's post hoc test. A p-value of less than 0.05 was considered to be statistically significant.

3. Results

3.1 Optimization of the LPCCD

'One-step' formation of nanoparticles with encapsulated Dox and Cur was achieved using the ethanol injection method. The concentration of $CaCO_3$, and the PAA/DOTAP and EPC/DOTAP weight ratios were optimized based on the characteristics of the nanoparticles and the loaded drug content.
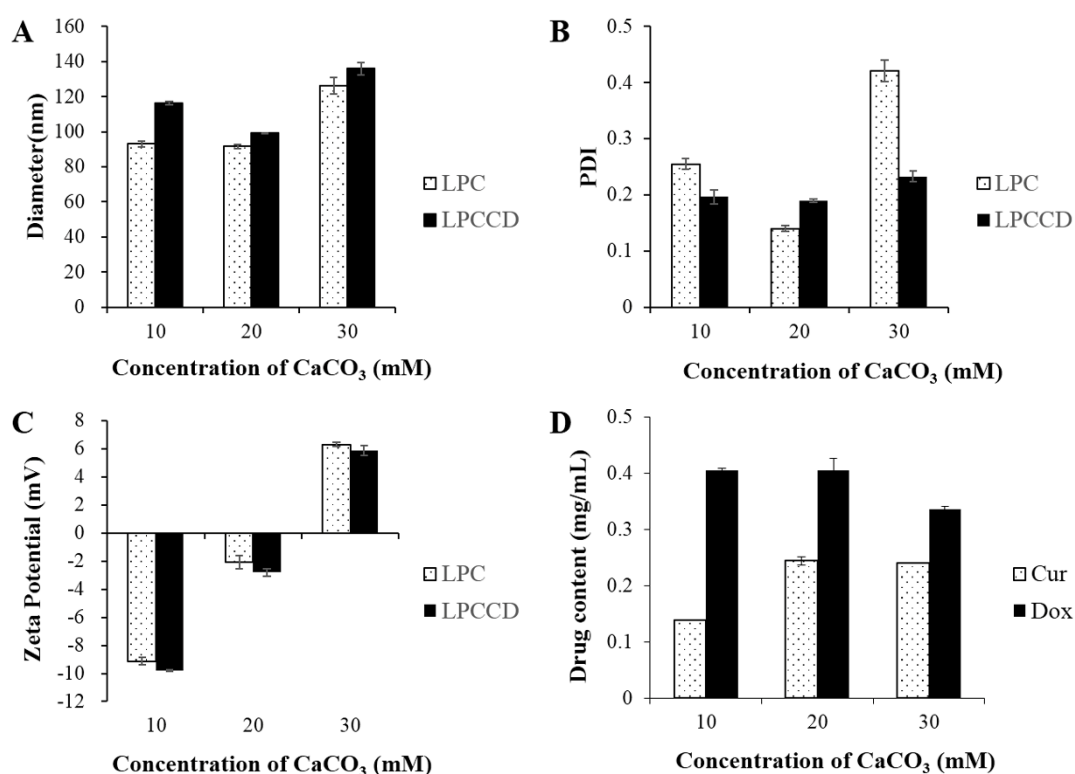
Fig. 1 **(A) Diameter, (B) PDI, (C) ζ potential of LPCCD and LPC, and (D) Cur and Dox drug content in LPCCD with variation of the concentration of $CaCO_3$.**
Each bar represents the mean ± S.D. of at least three experiments.

The diameter of the nanoparticles prepared using various concentrations of $CaCO_3$ was approximately 100 nm (**Fig. 1A**). As the concentration of $CaCO_3$ increased, a charge reversal was observed in the ζ potential (**Fig. 1C**). At 20 mM of $CaCO_3$, both Cur and Dox exhibited the highest level of encapsulation (**Fig. 1D**). Given that the smallest diameter and PDI (**Fig. 1A and C**) were detected at 20 mM of $CaCO_3$, this concentration of $CaCO_3$ was used in the following experiments.

In terms of the PAA/DOTAP weight ratio (**Fig. 2**), the diameter of both the LPC and the LPCCD was less than 100 nm, except for the LPCCD prepared at 16:5, while poor monodispersity was shown at a low weight ratio (4:5). Charge reversal was observed on the addition of PAA. The ζ potential of the nanoparticles decreased after Dox encapsulation. The highest Dox encapsulation was achieved at a PAA/DOTAP weight ratio of 8:5. Moreover, increased PAA restricted the encapsulation of Cur. Therefore, at a PAA/DOTAP weight ratio of 8:5, the balance in nanoparticle size, PDI and drug content was the best.
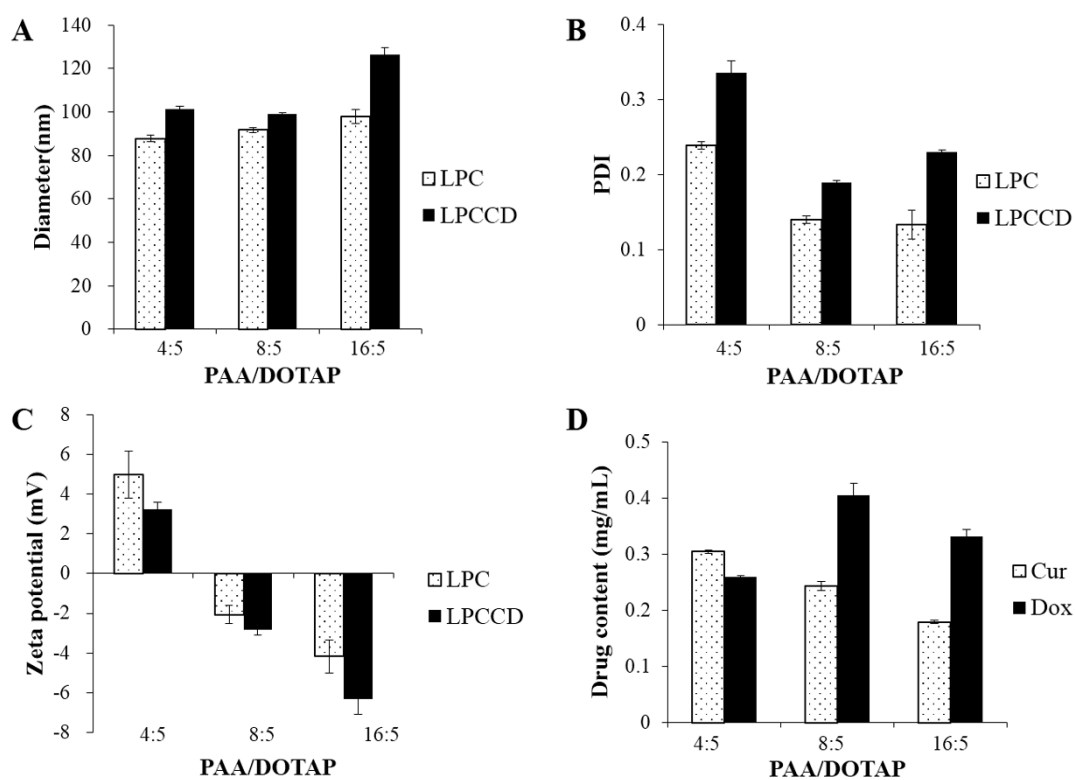
Fig. 2 **(A) Diameter, (B) polydispersity index, (C) ζ potential of LPCCD and LPC, and (D) Cur and Dox drug content in LPCCD with varied PAA/DOTAP weight ratios.**
Each bar represents the mean ± S.D. of at least three experiments.

Next, I optimized the EPC/DOTAP weight ratio (**Fig. 3**). Nanoparticles less than 100 nm in diameter were achieved at an EPC/DOTAP weight ratio of 4:1. The PDI tended to increase at higher ratios of EPC/DOTAP. Cur encapsulation was the best at an EPC/DOTAP weight ratio of 4:1. As the EPC/DOTAP weight ratio increased to 6:1, Dox encapsulation greatly decreased. Therefore, taking the characteristics of the nanoparticles

and the drug contents into consideration, the LPCCD prepared at an EPC/DOTAP weight ratio of 4:1 were optimal.
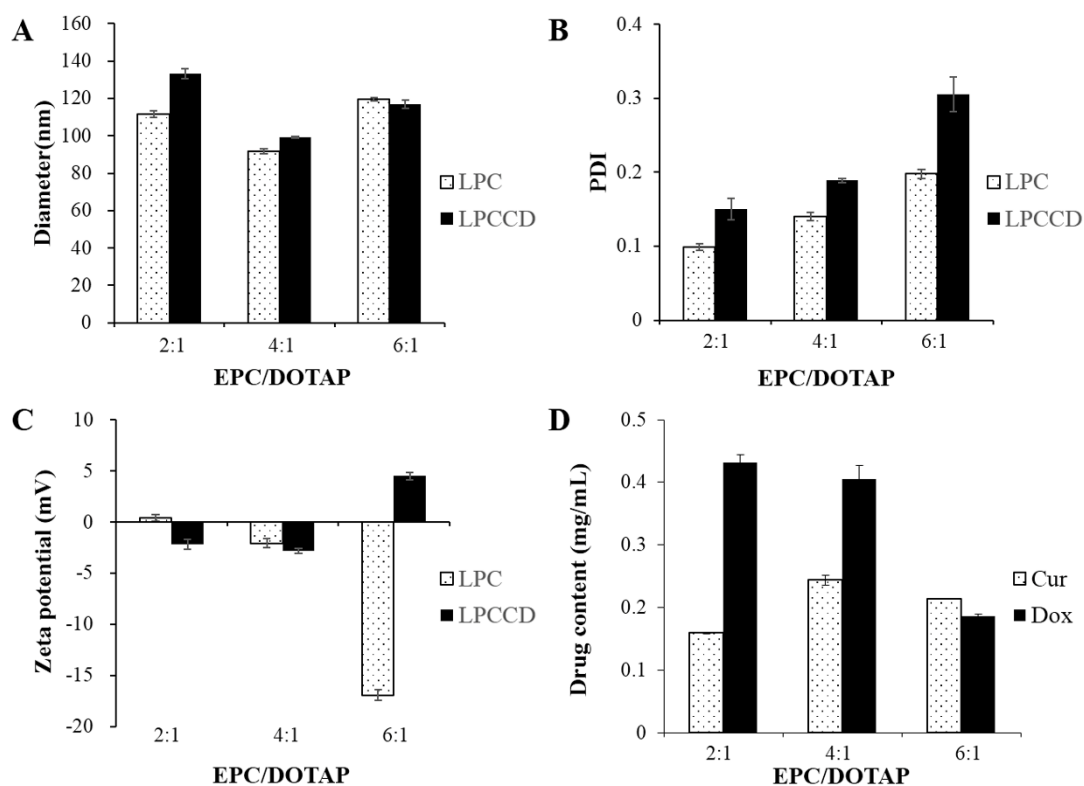
Fig. 3 **(A) Diameter, (B) polydispersity index, (C) ζ potential of LPCCD and LPC and (D) Cur and Dox drug content in LPCCD with varied EPC/DOTAP weight ratios.**
Each bar represents the mean ± S.D. of at least three experiments.

3.2 Characterization of the LPC and LPCCD

Under the optimized conditions, the diameters of both LPC and LPCCD were less than 100 nm with a reasonable monodispersity (**Table 1**). The encapsulation efficiency of both Dox and Cur was higher than 80% showing a molar ratio of Dox/Cur of approximately 1:1 (**Table 2**). Next, I measured the UV spectrum of Dox and Cur in the LPCCD (**Fig. 4**). It was clear that the characteristic peak of Cur around 430 nm overlapped with that of the LPCCD. However, one of the Dox characteristic peaks around 250 nm shifted to the left side of the curve of the LPCCD and the other Dox peaks around 500 nm decreased.

Table 1   Diameter, PDI and ζ potential of LPC and LPCCD

Group	Diameter (nm)	PDI	ζ potential (mV)
LPC	91.73 ± 1.15	0.140 ± 0.005	-2.07 ± 0.46
LPCCD	99.17 ± 0.31	0.189 ± 0.003	-2.82 ± 0.28

Results are expressed as the mean ± S.D. of three experiments.

Table 2   Drug content, drug loading (DL) and encapsulation efficiency (EE) of LPCCD

Drug	Content (mg/mL)	DL(%)	EE(%)
Dox	0.405 ± 0.022	2.59 ± 0.14	80.95 ± 4.33
Cur	0.244 ± 0.008	1.58 ± 0.05	81.37 ± 2.64

Results are expressed as the mean ± S.D. of three experiments.
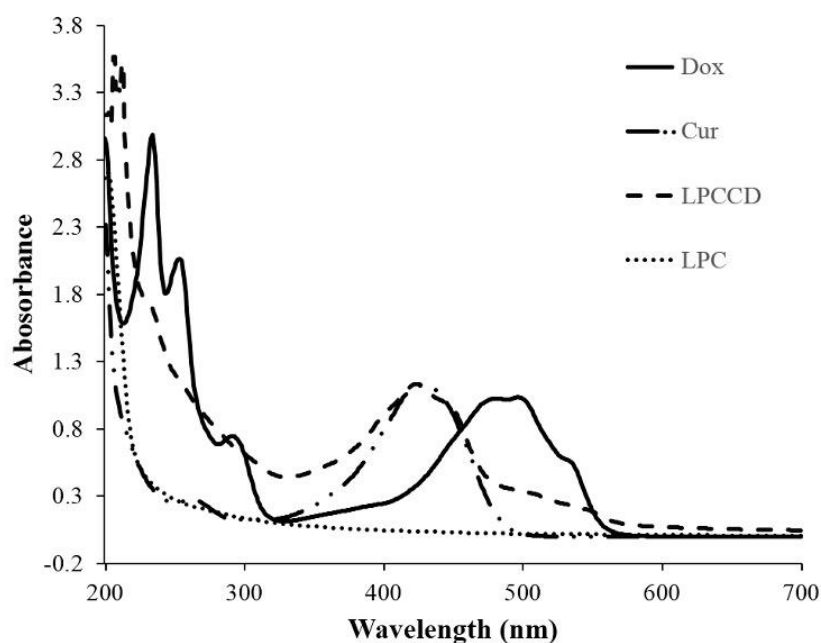
Fig. 4   UV spectrum of Dox, Cur, LPC and LPCCD.

3.3 pH sensitivity and stability of the nanoparticles

DDSs with pH sensitivity are promising for efficient intracellular drug release. The variation of the particle size distributions of both LPC and LPCCD when mixed with

buffer solutions at different pH values might indicate a morphological change in the nanoparticles (**Fig. 5**). In particular, the curve at pH 5.5 in LPCCD sample shifted slightly to the right and the intensity decreased.
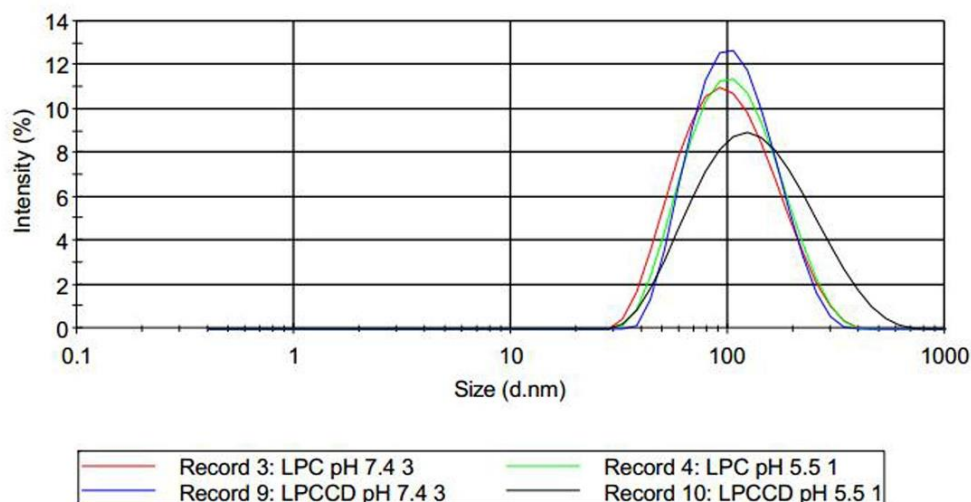
Fig. 5   **Particle size distributions of LPC and LPCCD in 0.01 M pH 7.4 Hepes buffer and 0.01 M pH 5.5 Mes buffer.**

The drug release behavior at different pH values was also studied. Both Dox and Cur release exhibited a noticeable sensitivity to pH, which was particularly marked for Dox release (**Fig. 6A**). As the pH decreased from 7.4 (physiological conditions) to 5.5 (lysosome/endosome environment), a sharply increased release of Dox was observed. However, Cur showed a delayed release at pH 5.5 compared with Dox. In addition, the release behavior of both Dox and Cur in the presence of 10% FBS was indistinguishable from that in the samples without FBS (**Fig. 6B**).
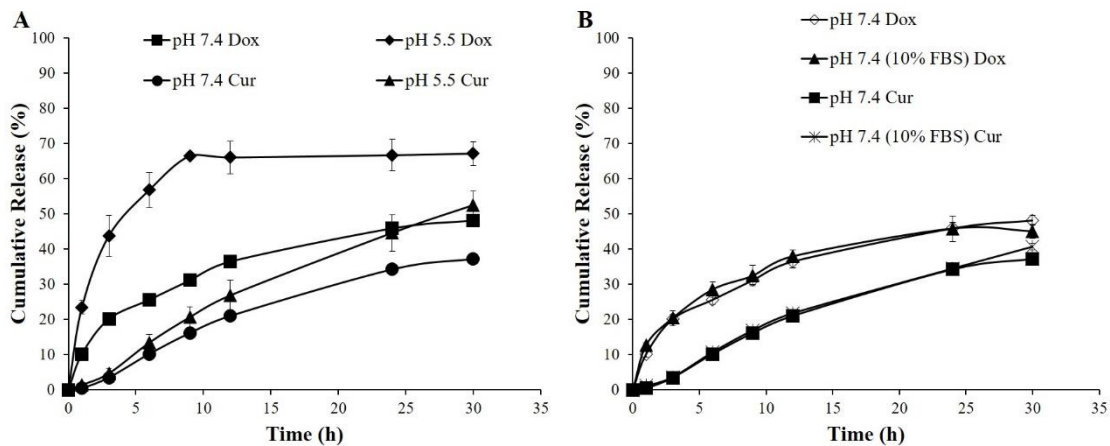
Fig. 6   Drug release behavior of Dox and Cur. (A) pH-sensitive drug release from LPCCD in 0.01 M pH 7.4 Hepes buffer (including 0.1% Tween 80) and 0.01 M pH 5.5 Mes buffer (including 0.1% Tween 80). (B) LPCCD alone or mixed with 10% FBS in 0.01 M pH 7.4 Hepes buffer (including 0.1% Tween 80).

Each symbol represents the mean ± S.D. of at least three experiments.

3.4 Evaluation of the cellular uptake of the LPCCD

Both Dox and Cur possess fluorescence that can be used to specify their intracellular distribution. Using confocal microscopy, Dox was clearly observed to enter the nuclei in the free drug groups, while the fluorescence of Cur was undetectable (**Fig. 7**). In the case of the LPCCD groups, the cellular uptake of both of Dox and Cur increased along with time until 8 h, at which apoptosis might occur as indicated by nuclear perforations. The released Dox overlapped with Cur, which was indicated by a yellow color. It was clear that LPCCD enhanced the cellular uptake of Cur into the cytoplasm. And, the accumulation of Dox in the nucleus might have resulted from pH-sensitive drug release from LPCCD. However, the cellular uptake and nuclear penetration of Dox in the LPCCD groups was not as good as in the free drug groups. The quantitation of cellular uptake was conducted using a flow cytometer, and it was demonstrated that the mean fluorescence intensity of cells treated using LPCCD was approximately half that of the free drug groups (**Fig. 8**).
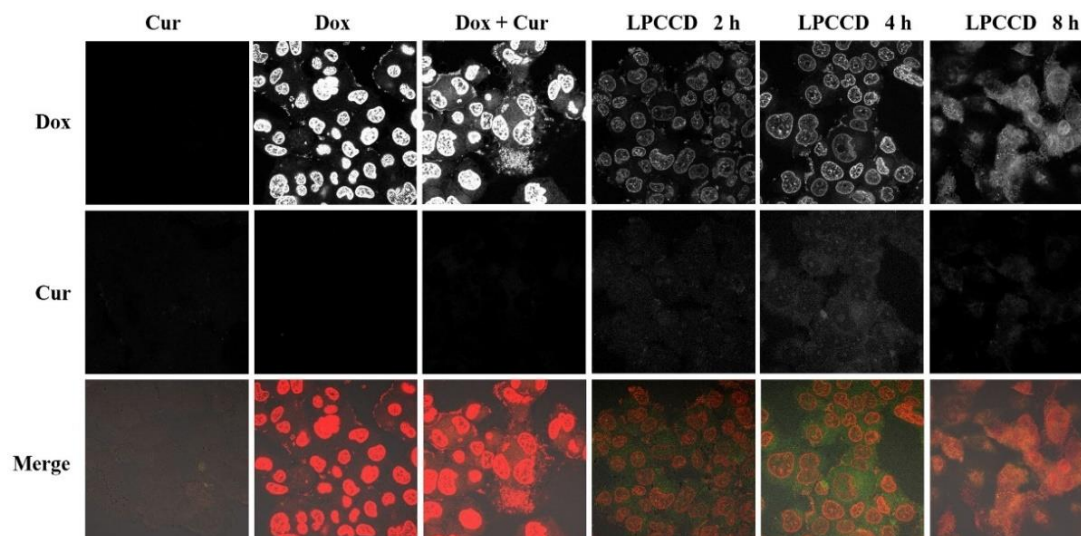
Fig. 7   Cellular uptake of free Cur, free Dox and free Dox + Cur at 2 h, and LPCCD at 2, 4 and 8 h, observed using confocal microscopy (at an equivalent concentration of Dox of 10 μM). Green: Cur, Red: Dox.

Group	Blank	Dox	Dox+Cur	LPCCD
MFI	4.35	16.2	16.9	9.03
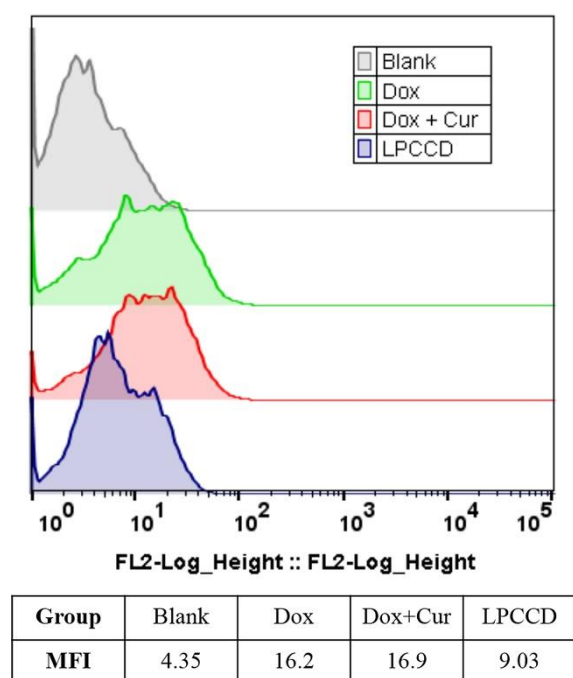
Fig. 8   Cellular uptake of free Dox, free Dox + Cur and LPCCD at 4 h, as detected using a flow cytometer (at an equivalent concentration of Dox of 10 μM).

3.5 Cytotoxicity and safety of the nanoparticles

An *in vitro* cell-growth inhibition study was performed using HepG2 cells (**Fig. 9**). At a low concentration of Dox, the inhibitory effect of the free Dox and LPCCD groups

on cell growth was slightly inferior to that of the free drug combination group. As the drug concentration increased, LPCCD exhibited higher cytotoxicity compared with Dox and Dox + Cur groups (**Fig. 9A**). The IC_{50} of Dox, Dox + Cur and the LPCCD was 0.1645, 0.0491 and 0.1256 μM, respectively. The LPC blank carrier produced no inhibitory effects on the growth of tumor cells at corresponding concentrations of EPC (**Fig. 9B**). A burst release of Ca^{2+} ions could affect the stability of erythrocytes. However, no significant levels of hemolysis were produced by neither the LPC nor liposomes prepared without PAA and $CaCO_3$ (**Fig. 10**). Even at the highest concentration of total lipid, the hemolysis was below 5% and the nanoparticles were deemed to possess no hemolytic activity *in vitro*. This result was consistent with no quick release of Ca^{2+} ions from LPCCD under physiological condition (**Fig. 6**). Therefore, the nanoparticles were suitable for an *in vivo* study.
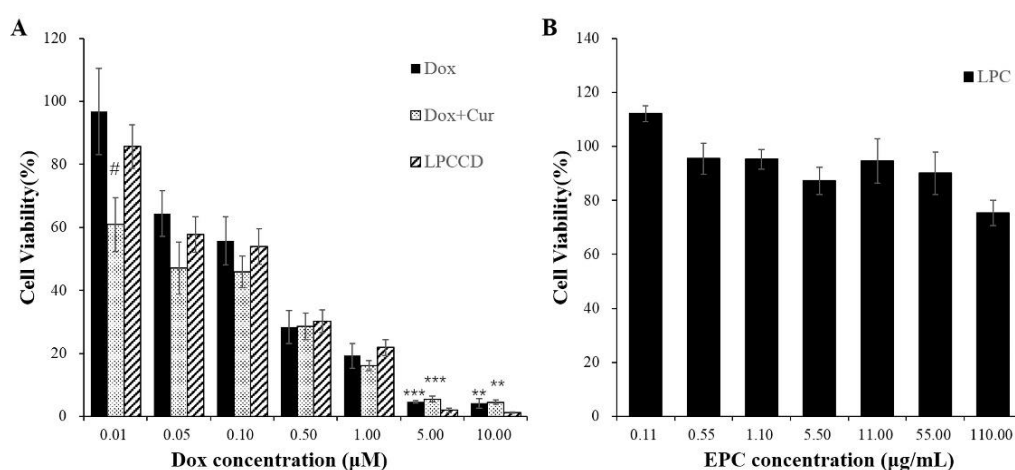
Fig. 9   Cytotoxicity of (A) free Dox, free Dox + Cur, LPCCD and (B) LPC, as detected using cell counting kit-8.

Each bar represents the mean ± S.D. of at least three experiments. Significant differences from LPCCD and free Dox group are represented as **$p<0.01$, ***$p<0.001$ and #$p<0.05$, respectively.
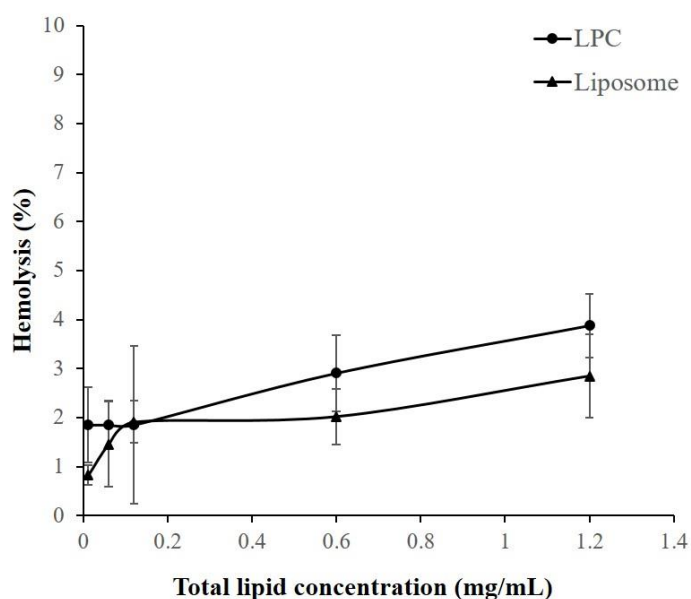
Fig. 10   **Hemolysis activity of Liposome (prepared without PAA and CaCO$_3$) and LPC at different total lipid concentrations.**

Each symbol represents the mean ± S.D. of at least three experiments.

3.6 Bio-distribution of Dox and Cur in mice

I checked the prolonged blood circulation of LPCCD in ddY mice (**Fig. 11**). LPCCD significantly increased the blood concentration of Dox and Cur at 3 h as compared with the free drug combination group (**Fig. 11A and D**). The accumulation of Dox and Cur in the spleen from delivered LPCCD was significantly increased compared with the free drug combination group (**Fig. 11B and E**). In the liver, lung and kidney, both Dox and Cur showed decreased distribution. Meanwhile, an obviously reduced distribution of Dox to the heart from the delivered LPCCD was observed in comparison with Dox in the free drug combination group. Distribution patterns of Dox and Cur in LPCCD group indicated apparently different accumulations between Dox and Cur, especially in the spleen and lung. This implied that a part of LPCCD were broken during blood circulation and subsequently released Dox and Cur partitioned from blood to tissues. As clearly shown from the obtained tissue/plasma ratios, nanoparticle formulation greatly decreased the partition of Dox and Cur from plasma to tissue (**Fig. 11C and F**). It was reasonable to conclude that the LPCCD avoided the fast clearance of drugs in circulation and altered the bio-distribution of Dox and Cur *in vivo*.
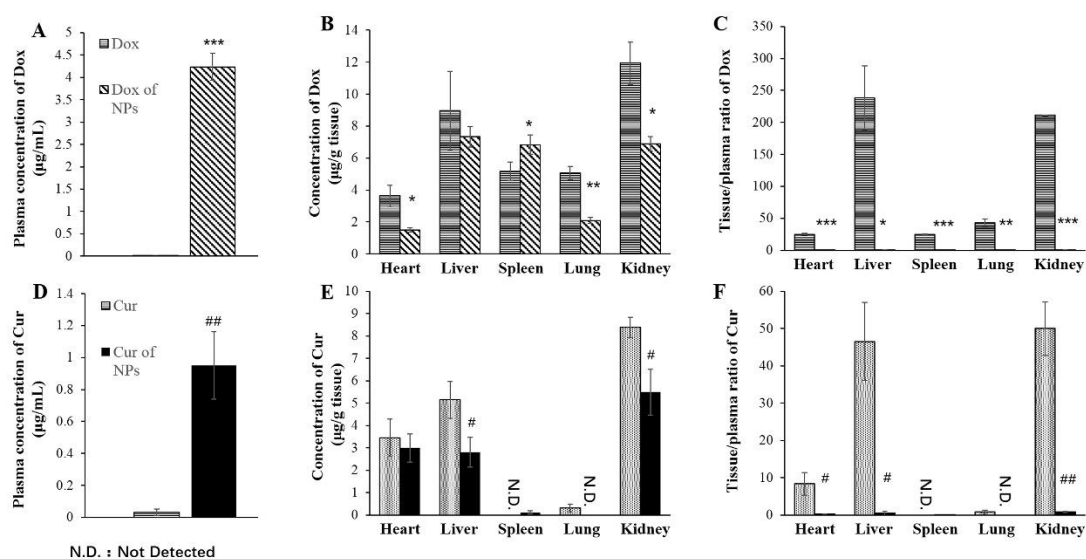
Fig. 11 Bio-distribution of Dox and Cur in (A, D) blood and (B, E) organs, and (C, F) tissue/plasma ratios after intravenous administration of Dox + Cur and LPCCD in mice.
Each bar represents the mean ± S.D. of at least three experiments. Significant differences from Dox + Cur group were represented as $*p<0.05$, $**p<0.01$, $***p<0.001$ for Dox and $\#p<0.05$, $\#\#p<0.01$, $\#\#\#p<0.001$ for Cur. N.D.: Not Detected.

3.7 Evaluation of the cardiotoxicity induced by Dox

A histological assay was performed for heart cryosections to evaluate Dox-induced cardiotoxicity. The morphology of the tissue was observed by light microscopy after H&E staining on cross-sections of the cardiac tissue (**Fig. 12**). Normal tissue morphology was observed in the saline group. A number of cells with significant edema are indicated using black arrows in the free Dox-treated group, indicating inflammation after continuous dosages. In addition, hypertrophic cardiac cells, identified from their elongated nuclei, were revealed in the free Dox-treated group (white arrows). In contrast, no inflammatory cells or hypertrophic cardiac cells were observed in the LPCCD group at an equivalent dose of Dox.
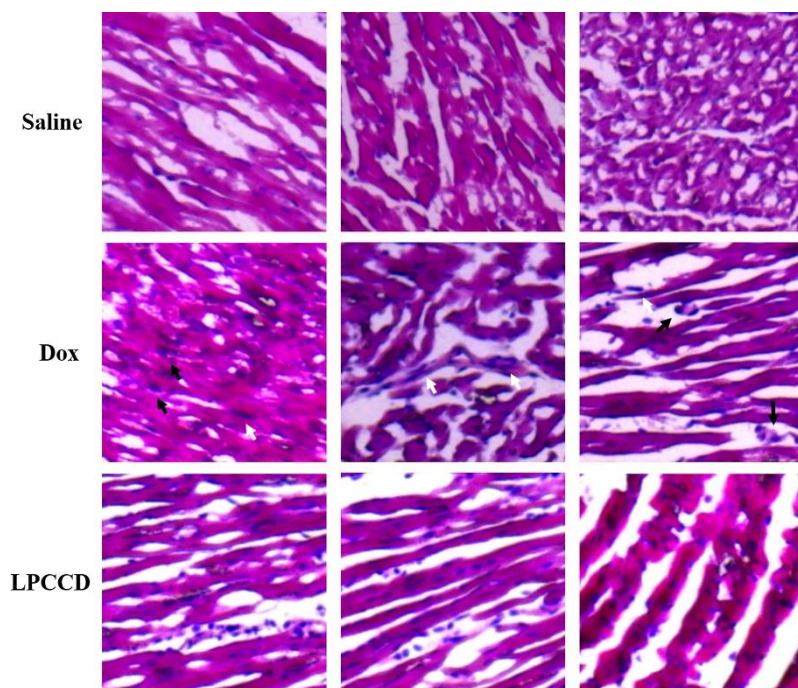
Fig. 12   Histopathological study on the cardio-toxicity of the mice treated with saline, free Dox and LPCCD.

The presence of hypertrophic cardiac cells was pointed out by white arrows and large edema was pointed out by black arrows.

4. Discussion

Combination therapy, with its obvious advantages, has been generally employed as a therapeutic regimen for cancer treatments. The sole use of Dox, a widely applied chemotherapeutic drug in clinical treatment, is associated with the development of MDR and cardiotoxicity problems. Preclinical research has shown that combining Dox with Cur, which possesses promising pharmacological effects, can overcome the setbacks of Dox alone [16]. A significant amount of research has been dedicated to harnessing the synergistic effects of this combination therapy in tumor inhibition. Micelles, nanocapsules and liposomes with functional components have been developed to achieve efficient co-delivery of Dox and Cur [7, 17, 18]. However, multi-step methods for nanoparticle preparation and drug encapsulation were involved. Therefore, I have developed a simplified method for the simultaneous encapsulation of Dox and Cur within 'one step', resulting in the LPCCD nanoparticles. The key point for the 'one-step' formation of the

LPCCD was utilization of the phenomenon that $CaCl_2$ is soluble in ethanol. Addition of $CaCl_2$ into the ethanol phase with other components including lipids, Dox, and Cur enabled us to form lipid/polyanion/$CaCO_3$ ternary nanoparticles containing drugs using the ethanol injection method. Therefore, the formation of highly organized LPCCD was successfully achieved within 'one step'.

It has been previously reported that the complexation of PAA/Dox resulted in nanoparticles with a diameter ranging from 600 to 900 nm that possessed a pH dependent interaction, and smaller nanoparticles of approximately 200 nm were obtained after mixing them with liposomes [13]. Enlightened by this study, I involved the PAA/Dox unit in the LPCCD system. In terms of Cur encapsulation, liposomes are a good choice. Therefore, the LPCCD co-delivery system was developed based on the triple complexation of lipid/Cur, PAA/Dox and $CaCO_3$. To decrease the particle size of the nanoparticles and improve the Dox loading, a high molecular weight PAA (25 kDa) was chosen. Given that interaction between PAA/Dox complexes and lipids would affect the stability of the lipid bilayer and monodispersity of the final ternary system, the 'one-step' formation method with both encapsulated Dox and Cur was developed and optimized. Importantly, the use of a certain amount of the DOTAP positive lipid in addition to the EPC neutral lipid was the key factor in achieving a successful 'one-step' formation.

During the optimization of the formation conditions of the LPCCD, the concentration of $CaCO_3$, and the PAA/DOTAP and EPC/DOTAP weight ratios were crucial factors in determining the particle size, PDI, and drug content. Increasing the concentration of $CaCO_3$ during the formation of the LPCCD caused the changes in surface charge from negative to positive (**Fig. 1C**). The charge neutralization of PAA by the Ca^{2+} ion might be a reason. The Cur content decreased at 10 mM $CaCO_3$. A strong electrostatic interaction between polyanion PAA and the lipid bilayer containing the DOTAP cationic lipid might interfere with the insertion of Cur. A specific concentration of the Ca^{2+} ion was required for efficient drug loading of Cur. However, too high concentration of $CaCO_3$ might inhibit the stable formation of the nanoparticles. In fact, 30 mM $CaCO_3$ resulted in increased PDI

(**Fig. 1B**) and flocculation (data not shown). A reduced encapsulation of Dox in the LPCCD at 30 mM $CaCO_3$ was observed, possibly because of the filtration through a filter. The electrostatic interactions between PAA and DOTAP played a key role in the formation of the nanoparticles (**Fig. 2**). Increasing the PAA/DOTAP ratio decreased the ζ potential, indicating that the surface of the nanoparticles was covered with PAA possessing carboxyl groups. Because Dox incorporation into the nanoparticles unexpectedly decreased the ζ potential despite the cationic charge of Dox, the interaction between PAA and Dox might inhibit the penetration of the PAA/$CaCO_3$/Dox complexes into the core of the lipid nanoparticles, resulting in a partial shift of PAA to the surface of the nanoparticles. Drug encapsulation was closely related to the PAA/DOTAP ratio. Charge balance and electrostatic interaction among PAA, DOTAP and Dox are important for the encapsulation of Dox. Increasing the PAA ratio decreased Cur encapsulation because of the interaction with DOTAP. There was no doubt that the lipid component proportions (EPC/DOTAP ratio) were closely related with the characteristics of the nanoparticles (**Fig. 3**). An increased amount of total lipid and the proportion of EPC increased the difficulty in the formation of the nanoparticles, especially via a 'one-step' formation method. The increased weight ratio of EPC/DOTAP gave rise to a decreased positive charge density of the LPC. Both sharply reduced encapsulation of Dox and the increased PDI might be caused by the loss of large-sized LPCCD nanoparticles during filtration. In general, strong negative and positive surface charge stabilize nanoparticles. This was in consistent with the properties of the LPCCD, since the particle size and PDI tended to be smaller when the ζ potential of the nanoparticles was approximately neutral. The formulation of LPCCD was complicated that contains several cations and anions. As cations, Dox, DOTAP and Ca^{2+} ions would interact with anions PAA and the CO_3^{2-} ions. If I assume that nanoparticle intermediates are present, the strong negative and positive charge of the intermediates undergo charge neutralization from free cations and anions, respectively, and as a consequence the intermediates become large. To produce the stable and small nanoparticles with a good drug loading efficiency, I determined the optimal concentration

of CaCO$_3$, and the optimal PAA/DOTAP and EPC/DOTAP weight ratios, which were 20 mM, 8:5, and 4:1, respectively.

Under optimal conditions, the particle size of the nanoparticles was less than 100 nm, indicating their successful preparation (**Table 1**). The nanoparticles contained a sufficient amount of Dox and Cur (**Table 2**). The encapsulation efficiencies for Dox and Cur were very high (**Table 2**). The encapsulation of Dox and Cur in the LPCCD was verified by recording their UV spectrum (**Fig. 4**). The characteristic Dox peak around 500 nm decreased, whereas the peak around 250 nm shifted to the left. This might be caused by a difference in the ionization condition of Dox through neutralization with PAA and the CO$_3^{2-}$ ion. Under an acidic environment, the disruption of CaCO$_3$ and the dissociation of the Dox/PAA/CaCO$_3$ complexes would occur. Therefore, a change in pH might influence the stability of the LPCCD (**Fig. 5**). Consistent with the size variation, both dissociation of the PAA/Dox complexes and the destruction of the CaCO$_3$ enhanced the drug release (**Fig. 6A**). Increased free Ca^{2+} ions might contribute to the enhanced Dox release by competitively inhibiting interaction with PAA. In the case of Cur, the dissociated PAA might combine with DOTAP to affect the stability of the lipid bilayer leading to a retarded release of Cur. Since the drug release was similar in 10% FBS (**Fig. 6B**), it is rational to suppose that the LPCCD can remain stable during *in vivo* circulation.

In the development of liposomes, pH-sensitive drug release has been pursued because of the stability of liposomes leading to a slow and incomplete drug release. Encapsulation of calcium phosphate and calcium carbonate during the formation of liposomes and nanoparticles has resulted in an impressive pH sensitivity and improved drug delivery [19, 20]. In the lysosome/endosome, low pH promotes an increase of calcium and bicarbonate/carbonate ions, the resulted osmotic swelling leading to a fast release of drugs into the cytoplasm [21]. To date, the delivery of DNA via liposomes in the presence of calcium phosphate and calcium carbonate was particularly intriguing in view of enhancing transfection efficiency [10, 22]. Based on the structural similarity between PAA and DNA in terms of the presence of abundant amounts of anion groups, I hypothesized

that it would be possible to form the co-precipitates of Ca^{2+}, Dox, PAA, CO_3^{2-}, and phospholipids with pH-sensitive drug release. In the current study, the optimization of the formulation clearly showed that the ratio between PAA, lipid and $CaCO_3$ was closely related with the characteristics of the formed nanoparticles and the drug loading. An obvious pH-sensitive drug release was observed for both Dox and Cur (**Fig. 6A**). Not only the pH sensitivity in the interaction between PAA and Dox, but also the destruction of $CaCO_3$ under an acidic environment might promote the burst release of Dox. Simultaneously, because of the electrostatic interaction between PAA and DOTAP-containing lipid bilayer, disruption of the PAA/Dox/$CaCO_3$ complexes at pH 5.5 resulted in instability in the lipid bilayer, promoting a delayed release of Cur.

To guarantee the stability and monodispersity of the LPCCD nanoparticles, a certain amount of PEGylated lipid DSPE-PEG was necessary to prevent aggregation during the 'one-step' formation that involved complex electrostatic interactions among multiple components. The peripheral PEG moieties imparted stability to the LPCCD in the presence of FBS (**Fig. 6B**) and safety in terms of hemolysis (**Fig. 10**). In addition, the blood circulation of the LPCCD was also greatly prolonged due to the PEG coating that prevented phagocytosis by the reticuloendothelial system (**Fig. 11**). However, DSPE-PEG is a double-edged sword. A high ratio of DSPE-PEG in a lipid bilayer might suppress the cellular uptake of LPCCD, as potentially indicated by the reduced accumulation of Dox (**Figs. 7 and 8**). The cytotoxicity of LPCCD on tumor cells was slightly inferior to the free drug combination group (**Fig. 9**). However, LPCCD enhanced the cytotoxicity in comparison of free Dox group, despite a significantly reduced cellular uptake of Dox. This may be the result of increased cellular uptake of Cur from the LPCCD, indicating synergistic effect of Dox and Cur. It is reasonable to suppose that the LPCCD promotes the antitumor effects of Dox and Cur via efficient co-delivery. For future tumor-selective delivery of LPCCD, the incorporation of tumor-specific ligands will be required.

The realization of the synergistic effects of combination therapies relies on the efficient co-delivery of drugs to targeted tissues. Generally, the *in vivo* bio-distribution

behaviors of multiple drugs are diverse because of the distinction of characteristics such as lipophilicity, protein binding and metabolic pathway. With the employment of nanoparticles, the component drugs are capable to achieve desired spatiotemporal distribution *in vivo*. As shown in **Fig. 11**, the altered bio-distribution of both Dox and Cur in the LPCCD group compared with the free drug combination group was observed in mice. LPCCD increased plasma concentration and exhibited similar tissue-distribution of the Dox and Cur *in vivo*, providing a foundation for the realization of synergistic effect of the combination therapy. In addition, the decreased distribution of Dox to the heart in the LPCCD group was consistent with ameliorated cardiotoxicity (**Fig. 12**). Therefore, I expect that the co-delivery of Dox and Cur using LPCCD would be an effective DDS with high safety.

5. Conclusion

I have successfully developed a $CaCO_3$-encapsulated PAA-stabilized lipid ternary system for Dox and Cur combination therapy. With the use of polyanion-PAA and $CaCO_3$, the LPCCD co-delivery system was achieved using a 'one-step' formation method and it possesses a robust pH-sensitive drug release. A narrow size distribution of nanoparticles of approximately 100 nm in diameter was achieved. The encapsulation efficiencies of Dox and Cur in the LPCCD were high. Moreover, the LPCCD produced significant cytotoxicity in tumor cells and decreased cardiotoxicity compared with free Dox. In summary, the LPCCD nanoparticles have potential in cancer therapy and this ternary system is promising for further application with other chemotherapeutic combination therapies.

Chapter II Targeted co-delivery of protein/drug combinations by lipid-based calcium carbonate nanoparticles to colon cancer

1. Introduction

Combination therapies have been widely used in clinical treatments for many refractory diseases with complex nature [23, 24]. The combination therapies such as chemotherapeutic combinations, nucleic acid-based gene therapies and bio-macromolecule-assisted strategies are promising in improving the therapeutic outcomes, ameliorating side effects and overcoming the multi-drug resistance in cancer treatment [25-27]. Despite the promise of improved clinical treatments by the combination therapies, the lack of proper drug delivery systems (DDSs) may not guarantee the spatial and temporal consistency of the combinations in the bio-distribution *in vivo*. Numerous DDSs based on lipids, polymers and inorganic materials for the effective encapsulation and delivery of combination therapies have been reviewed including combinations of small-molecular chemodrugs and siRNA (or DNA) [28]. The co-delivery by a single carrier was aiming at synergistic effects on treatments. In Chapter I, I have formulated a lipid-based ternary system for the doxorubicin/curcumin combination therapy with a 'one-step' preparation method. The nanoparticles improved the blood concentration and changed the bio-distribution of encapsulated doxorubicin and curcumin compared with the free combination group after intravenous administration.

Nowadays, because more and more therapeutic proteins (such as insulin, monoclonal antibodies, chimeric proteins, etc.) were used in the clinical treatment [29], a flurry of protein/small-molecular drug combinations had been developed acting on multiple targets. Compared with the small-molecular drug, proteins possessed the specific, folded and three-dimensional structure that is more challenging in maintaining the activity during delivery *in vivo*. Nanocarriers are capable to protect proteins from degradation and denaturation, promoted the systemic circulation time [30]. The therapeutic proteins are

validated to act not only outside of the cells including the plasma membranes but also inside of the cells. In the development of the protein/drug combinations, the co-delivery systems were generally prepared as drug-encapsulated nanoparticles with proteins inserted on the periphery to act on the cell surface. For example, a membrane-associated cytokine TRAIL (tumor necrosis factor-related apoptosis-inducing ligand) has been attached outside of the doxorubicin-loaded graphene nanoparticles [31]. Monoclonal antibodies were widely used in such combinations by conjugation to the nanoparticles as both therapeutic units and targeting moieties [32, 33]. However, single carrier with drug/protein which both are working in the cytosol has been rarely reported so far, while there are examples of sequential treatments including apoptin proteins/dacarbazine [34], apoptin proteins/paclitaxel/etoposide [35] and caspase-3/flavopiridol [36] combinations. Because of the major differences in the characteristics between biomacromolecules and small molecules, it is more challenging to co-encapsulate the protein/drug combinations in the single nanoparticles compared with the small-molecular drug combinations. Based on the former study of hybrid system for small-molecular drug combination, I improved the nanocarrier to realize the co-delivery of protein/drug combination which both are working in the cytosol.

Superoxide dismutase (SOD) is an antioxidant enzyme to catalyze the reaction from superoxide anion (O_2^-) to hydrogen peroxide (H_2O_2) that regulate the reactive oxygen species (ROS) level [37]. Tumor cells with 'hyper-metabolism' characteristic might generate abundant ROS from mitochondria and the endoplasmic reticulum [38]. Under certain circumstances, the elevated ROS levels promote the cell growth. Meanwhile, they can also induce apoptosis via proapoptotic signal molecules [39]. Alexis *et al.* found that the excessive H_2O_2 in the tumor cells with high level of ROS, such as CT26 colon tumor cells and Hepa 1-6 liver tumor cells, would surpass the range of proliferative ROS level and result in inhibition on the cell growth [40]. They evaluated the growth inhibition effects of several combinations of SOD mimics and chemotherapeutic drugs. The results showed that the SOD mimics and paclitaxel (PTX) combination showed an impressive inhibition

effect on the proliferation of CT26 colon tumor cells. Therefore, a SOD/PTX therapeutic combination was used in my study for inhibition of colon tumor cell growth. Besides, a fluorescently labeled protein BSA-FITC and a small molecule dye DiD were used as model protein/drug combination for the evaluation of cellular distribution and bio-distribution.

The electrostatic and hydrophobic interactions have been verified to contribute to the formation of protein/lipid nanocomplexes through a structure-function relationship study [41]. In general, the encapsulation of hydrophobic drugs into such lipid systems is based on hydrophobic interactions and hydrogen bonding among drugs, lipids and proteins. Therefore, I hypothesized that a mixture of cationic lipid/neutral lipid at a certain ratio could interact with proteins, subsequently forming the backbone of the nanoparticles. Calcium carbonate ($CaCO_3$) was widely used for the nanoparticles to facilitate the delivery of drugs and genes [8]. As a pH-sensitive stimuli unit in my nanocarrier [14], $CaCO_3$ with inherent pH sensitivity can be destroyed in the acidic environment and lead to promoted drug release. Polyelectrolytes was reported to act as the template for the formation of $CaCO_3$ via electrostatic interaction with Ca^{2+} ions [11]. Because proteins as a category of polyelectrolytes with abundant anionic moieties, I supposed that proteins could stabilize the $CaCO_3$ in this nanoparticle.

RGD peptides are known as selective ligands toward αvβ3 integrin that overexpressed on tumor neovasculature and tumor cells including melanoma, prostate cancer, breast cancer, colon cancer [42, 43]. Suga *et al.* have synthesized a lipid-RGD with serine-glycine repeats $(SG)_n$ [44] as a spacer and inserted in the liposome for the colon tumor growth targeting [45]. To endow the nanocarrier with targeting ability to tumor cells, the lipid-RGD was inserted in this lipid-based nanoparticle. Due to the coverage of broad spectrum of cancers and dual targeting to endothelial cell and tumor cells, the lipid-RGD unit was expected to enhance the accumulation of nanoparticles in the tumor region and promote the cellular uptake by tumor cells.

In the Chapter II, I succeeded in encapsulation of protein/drug combination and CaCO$_3$ within lipid-based nanoparticles via the 'one-step' preparation method. A lipid-RGD was post-inserted for improved uptake by colon tumor cells. The prescription was optimized on the ratios among lipids, proteins and CaCO$_3$ in consideration of the physicochemical properties of nanoparticles. Characterizations of nanoparticles, *in vitro* evaluation on the tumor cells and *in vivo* bio-distribution study on the mice were demonstrated. It was expected for the nanoparticles to achieve efficient co-delivery of both the protein and drug to tumor cells (**Fig. 13**).
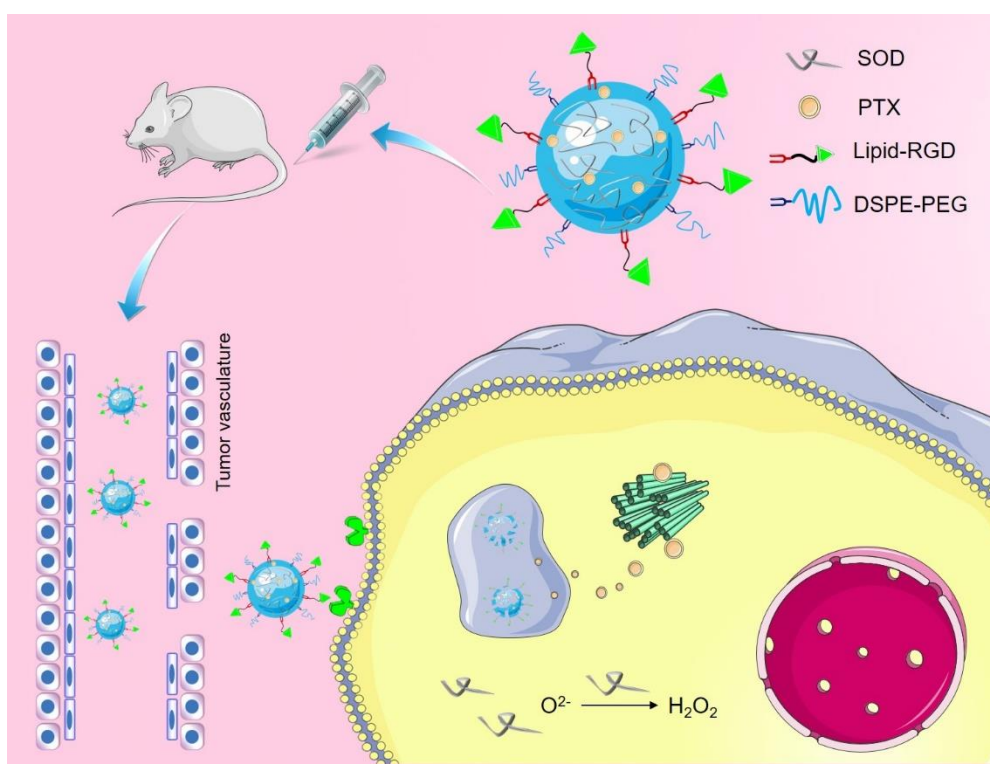
Fig. 13   Schematic illustration of composition, tumor targeting and pH-sensitive drug release of nanoparticles for the protein/drug combination therapy.

2. Materials and methods

2.1 Materials and reagents

Egg lecithin (EPC) and superoxide dismutase (SOD, Cu/Zn type, 40,000 U/mL) were purchased from Wako Pure Chemical Industries (Osaka, Japan). *N*-(Carbonyl-methoxypolyethylene glycol 2000)-1,2-distearoyl-sn-glycero-3-phosphoethanolamine

(DSPE-PEG$_{2000}$) and 1,2-dioleoyl-3-trimethylammonium-propane (DOTAP) chloride salt was obtained from NOF corporation (Tokyo, Japan). Paclitaxel (PTX) was provided by Tokyo Chemical Industry Co., Ltd. (Tokyo, Japan). Bovine serum albumin (BSA) were purchased from Sigma-Aldrich (St. Louis, MO, USA). The lipid-RGD ligand with serine-glycine repeats $(SG)_n$ repeat as a spacer synthesized via solid phase peptide synthesis method was kindly provided by Suga et al. [45]

The other inorganic chemicals were obtained from Nacalai Tesque (Kyoto, Japan). All organic solvents of analytical grade were purchased from Sigma-Aldrich (St. Louis, MO, USA). Water was prepared through Direct-Q UV (Merck Millipore, Merck KGaA, Darmstadt, Germany).

2.2 Cells and animals

Colon 26 murine colorectal cancer cell line was obtained from RIKEN (Tokyo, Japan). RPMI 1640 cell culture media were purchased from Wako Pure Chemical Industries (Osaka, Japan).

Male ddY mice (25–27 g) supplied by Japan SLC Inc. (Shizuoka, Japan) were fed with a standard laboratory diet and were housed at an ambient temperature and humidity in air-conditioned chambers before the experiments. All animal experiments were conducted in full compliance with the Guideline for Animal Experimentation at Nagasaki University.

2.3 Synthesis of BSA-FITC

The FITC-labeled BSA was prepared according to the previous reports [46]. Briefly, 1 mg/ml FITC-I (Dojindo, Kumamoto, Japan) in DMSO solution was added to 2 mg/ml of BSA in 0.1 M pH 9.0 sodium carbonate buffer dropwise under stirring. Then the solution was stirred in the dark for 20 hours at 4°C. After reaction, the unbound FITC was separated from the conjugate by ultrafiltration tube (MWCO 30 kDa, Vivaspin, Sartorius Stedim Biotech, Germany). The solution was centrifuged at $12,000 \times g$ for 5 min per once and replenished with water for three times. Purified BSA-FITC was stored at 4°C. The concentration of BSA-FITC was calculated in accordance with the following equation:

$$\text{Concentration (mg/mL)} = \frac{A_{280} - 0.35 \times A_{494}}{E^{0.1\%}} \times 100 \qquad\qquad 2\text{-}1$$

where A_{280} and A_{494} is the absorbance of BSA-FITC at 280 and 494 nm, and $E^{0.1\%}$ is the absorption of 1.0 mg/ml BSA at 280 nm (**Table 3**). The BSA-FITC was freshly prepared before use.

Table 3   The concentration of synthesized BSA-FITC

Batch	NO. 1	NO. 2	NO. 3
A_{280}	0.382	0.410	0.369
A_{494}	0.671	0.6124	0.546
Concentration (mg/mL)	11.148	14.823	13.477

2.4 Preparation and optimization of lipid-RGD inserted lipid/protein/drug/CaCO₃ nanoparticles

The preparation of nanoparticles with both encapsulated protein and drug was achieved by one-step ethanol injection method. Briefly, 100 μL of BSA or SOD water solution (10 mg/mL) was mixed with 400 μL of propylene glycol (PG), 30 μL of Na_2CO_3 water solution (0.2 M), 800 μL of EPC ethanol solution (20 mg/mL), 160 μL of DOTAP ethanol solution (10 mg/mL), and 40 μL of PTX ethanol solution (2.5 mg/mL) or DiD ethanol solution (2 mg/mL) in sequence as ethanol phase. The water phase was prepared by blending 1.4 mL 25% glucose solution, 1.28 mL DSPE-PEG water solution (5 mg/mL), 60 μL $CaCl_2$ water solution (0.2 M) and adjusted with water to the final ethanol phase/water phase ratio of 1:4 (v/v). Both ethanol phase and water phase were stirred for 15 min before mixing. Under stirring, the ethanol phase was added to water phase dropwise. After 1 h stirring at room temperature, the solution was centrifuged via an ultrafiltration tube (MWCO 100 kDa Amicon Ultra-15, Merck Millipore Ltd., Ireland). The alcohols were removed during this process with replenished 5% glucose to eventual 1 mL nanoparticles solution.

The RGD peptide-inserted nanoparticles were prepared via post-insertion method. After preparation of above nanoparticles, the lipid-RGD ligand (4 mg/mL) was added to the nanoparticles solution under 60°C water bath dropwise at a weight ratio of EPC/lipid-RGD = 12.5:1. The mixture was further incubated for 1 h, and the RGD-inserted nanoparticles were condensed through ultrafiltration tube (MWCO 100 kDa) to 1 mL in the similar fashion.

To evaluate the characteristics of the nanoparticles, different protein/drug combinations were encapsulated. For the study of cellular uptake and bio-distribution, lipid/BSA-FITC/DiD/$CaCO_3$ (LBDC) and RGD-inserted lipid/BSA-FITC/DiD/$CaCO_3$ (RLBDC) were prepared. To investigate the drug release behavior, RGD-inserted lipid /BSA-FITC/PTX/$CaCO_3$ (RLBPC) were prepared. And for the evaluation of anti-tumor efficacy, lipid/SOD/PTX/$CaCO_3$ (LSPC) and RGD-inserted lipid/SOD/PTX/$CaCO_3$ (RLSPC) were prepared.

2.5 Diameter and ζ potential of nanoparticles

A Zetasizer Nano ZS (Malvern, UK) was used to detect the diameter, PDI and ζ potential of the prepared nanoparticles. All the nanoparticles were 4 times diluted by 5% glucose before detection. Besides, the pH sensitivity of nanoparticles was investigated by the particle size detection. The LBDC were 4 times diluted by 0.01 M pH 7.4 Hepes buffer and 0.01 M pH 5.5 Mes buffer, respectively, and incubated for 3 h before detection.

2.6 SOD activity under processing condition

The activity of SOD enzyme is highly depended on the structural complexity that make them difficult to formulate. It is necessary to evaluate the effect of components, solvents and process condition during the preparation on the activity of SOD. SOD stock solution of 400 U/mL was prepared. SOD solution and the other components were added to the 1.5 mL microtube and incubated at various conditions (**Table 4**). After incubation for defined time, the activity of SOD was detected by a SOD Assay Kit (Dojindo, Kumamoto, Japan). The absorbance was measured at 450 nm using a microplate photometer (Multiskan™ FC, Thermo Fisher Scientific). The activity of SOD alone

solution at 4°C (NO.1 sample) was served as 100% and the activity of each sample was expressed as normalized value using NO.1 as control.

Table 4 Experimental conditions for effects of components, solvents and processing temperature during preparation on the activity of SOD.

NO.	Temp. (°C)	SOD (µL)	PG (µL)	Ethanol (µL)	Na_2CO_3 (µL)	$CaCl_2$ (µL)	H_2O (µL)	Time (h)
1	4	50	-	-	-	-	950	0
2	25	50	200	-	-	-	750	1
3	25	50	200	-	-	-	750	0.5
4	25	50	200	500	-	-	250	1
5	25	50	200	500	-	-	250	0.5
6	60	50	-	-	-	-	950	1
7	60	50	-	-	-	-	950	2
8	25	50	200	500	20	-	230	1
9	25	50	200	500	-	40	210	1

2.7 Drug content and encapsulate efficiency

The encapsulated PTX and SOD were determined via high performance liquid chromatography (HPLC) with a UV detector (SPD-10A, Shimadzu, Kyoto, Japan) and a SOD Assay Kit (Dojindo, Kumamoto, Japan), separately. For the determination of PTX, 20 µL of nanoparticles were added to 980 µL methanol and sonicated for 15 min. Then the solution was analyzed at $\lambda = 230$ nm using a mobile phase of water: acetonitrile = 40:60 (v/v). The content of SOD was represented by the enzymatic activity. According to a pre-determined activity curve (**Fig. 14**), the SOD concentration can be quantified by the linear curve. Briefly, 20 µL of nanoparticles were added to 980 µL 0.01 M pH 5.5 Mes buffer and incubated in 37°C water bath for 10 min. After 10 times diluted by the dilution buffer from the detection kit, the absorbance was measured at 450 nm.
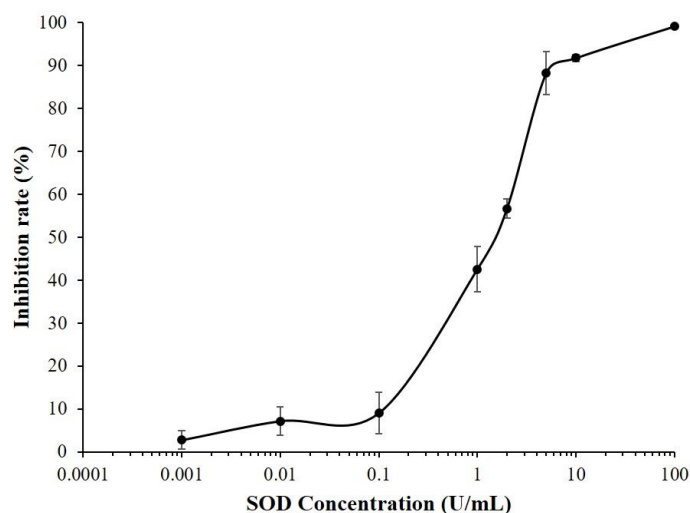
Fig. 14 SOD activity-concentration curve (activity was expressed as inhibition rate).
Each symbol represents the mean ± S.D. of at least three experiments.

The quantitation of BSA-FITC and DiD (Thermo Fisher Scientific) was implemented by a fluorescence spectrometer (RF-6000, Shimadzu, Kyoto, Japan). Twenty microliters of nanoparticles were added to 980 μL methanol and sonicated for 15 min. For the detection of BSA-FITC, the solution was 10 times diluted by the 0.1 M pH 9.0 sodium carbonate buffer. The ethanol was used to dilute DiD for 10 times in volume before detection. The excitation (Ex)/emission (Em) wavelength for BSA-FITC and DiD was 494/524 nm and 644/670 nm, respectively. Encapsulate efficiency (EE) was calculated in accordance with the following equation:

$$EE\,(wt.\%) = \frac{Weight_{load}}{Weight_{feed}} \times 100 \qquad\qquad 2\text{-}2$$

2.8 pH-sensitive drug release

RLBPC was prepared for the release study. Drug release behavior of both BSA-FITC and PTX encapsulated was monitored using an ultrafiltration method and a membrane dialysis technique, respectively. The physiological environment and lysosome/endosome microenvironment were simulated by 0.01 M pH 7.4 Hepes buffer and 0.01 M pH 5.5 Mes buffer, respectively. Besides, 0.1% Tween 80 was added to both media for the solubilization of PTX. For the detection of BSA-FITC, 200 μL of RLBPC was added directly to 9.8 mL mediums. In a shaking water bath at 37°C, 1 mL of solution was moved

to an ultrafiltration tube (MWCO 100 kDa) at certain intervals and centrifuged at 4,830 $\times g$ for 5 min. The flow-through solution was 5 times diluted by the 0.1 M pH 9.0 sodium carbonate buffer and detected by a fluorescence spectrometer. For the detection of PTX, 200 μL of RLBPC was placed into a dialysis bag (MWCO, 12 kDa) and exposed to 10 mL media. In a shaking water bath at 37°C, 100 μL of medium was withdrawn and the same amount of fresh medium was replenished. The amount of PTX was determined using HPLC.

2.9 In vitro cellular uptake

Colon 26 murine colorectal cancer cell was cultured in RPMI-1640 including 10% FBS, 100 U/mL penicillin and 100 μg/mL streptomycin at 37°C, 5% CO_2 and 90% relative humidity. The cellular uptake was observed by a confocal microscopy (LSM710, Carl Zeiss Microimaging GmbH, Jena, Germany). Briefly, the cells were seeded in glass-base dishes at a density of 1×10^5 cells/dish and pre-incubated for 24 h. Then, BSA-FITC + DiD, LBDC and RLBDC (final concentration of 14 nM of BSA-FITC and 0.88 nM of DiD) in RPMI-1640 medium (with FBS) were incubated with the cells at 37°C. After 3 h incubation, the supernatant was removed and washed with PBS. LysoTracker® Red (Thermo Fisher Scientific) in RPMI-1640 medium (100 nM) was added. After 10 min incubation, the supernatant was removed, washed by PBS, fixed with 4% paraformaldehyde in PBS for 15 min, and washed again. DAPI (Sigma-Aldrich) in RPMI-1640 medium (5 μg/mL) was added and incubated for 10 min before washing with PBS. Two drops of Slow Fade Diamond® (Thermo Fisher Scientific) were added and observed.

For the quantitation of cellular uptake of BSA-FITC and DiD, a fluorescence-activated flow cytometer (LSRfortessa X-20, Becton Dickinson, USA) was used to detect the fluorescence. To study the mechanism of cellular uptake, a RGD peptide-inserted liposomes (RLipo) were prepared [45]. The cells were seeded in a 24-well plate at a density of 1×10^5 cells/well and pre-incubated for 24 h. For the control group, RLBDC (final concentration of 14 nM of BSA-FITC and 0.88 nM of DiD) in RPMI-1640 medium (with FBS) were incubated with cells for 3 h. The Rlipo at a 20 times molar ratio of the lipid-

RGD inserted in the RLBDC were pre-incubated with cells for 30 min and then co-incubated with RLBDC at the same concentration of control group for another 3 h. The cells were washed with PBS, trypsinized and collected, then detected after resuspended in 0.5 mL of PBS.

2.10 In vitro cytotoxicity

The cytotoxicity of nanoparticles and blank carrier lipid/CaCO$_3$ (LC) and RGD inserted lipid/CaCO$_3$ (RLC) was evaluated on the Colon 26 cells by cell counting kit-8 (Dojindo, Kumamoto, Japan). The cells were seeded in 96-well plates at a density of 1×10^4 cells/well. After 12 h incubation, SOD, PTX, SOD + PTX, LSPC and RLSPC at various concentrations were added to the wells. 48 h incubation later, removed the solution in wells and washed with PBS. Then 10 µL of WST-8 in 100 µL RMPI-1640 was added to each well and incubated for another 1 h. The absorbance was measured at 450 nm using a microplate photometer (Multiskan™ FC, Thermo Fisher Scientific). Blank wells and untreated cells were served as negative and positive controls, respectively.

2.11 Determination of nanoparticles stability in FBS solution

The LBDC and RLBDC were added to the PBS solution containing 40% (v/v) FBS and incubated in a 37°C water bath. At defined time intervals, the samples were collected and ultrafiltrated (MWCO 100 kDa) at $4,830 \times g$ for 10 min. The solution of inner tube was added up to 1 mL with 5% glucose. The fluorescence of BSA-FITC and DiD were detected according to the method in "*2.7 Drug content and encapsulate efficiency*".

2.12 In vivo bio-distribution of the nanoparticles

The study was implemented on the ddY mice. BSA-FITC + DiD or LBDC were intravenously injected via the tail vein of mice at a BSA-FITC dose of 1.92 mg/kg. At the time points of 1, 6 and 24 h, the mice were anesthetized using a drug mix (butorphanol, medetomidine and midazolam). Blood was taken from the inferior vena cava and then the heart, liver, spleen, lung and kidney were harvested and weighed.

A tissue clearance method was developed to detect the concentration of fluorescence. For the detection of FITC-BSA, SeeDBp (80.2% w/v fructose with 0.5% α-thioglycerol in PBS, pH 8.5 adjusted by 1 M NaOH) [47] was employed. Briefly, organs were homogenized with PBS at 3 µL/µg for liver and 6 µL/µg for the other organs. The blood was centrifuged at $1,500 \times g$ for 15 min to receive the plasma. For the detection of BSA-FITC, 100 µL homogenates and 50 µL plasma were mixed with 10 µL 5% glucose and incubated at 37°C for 30 min. Then SeeDBp (pH 8.5) were added up to 500 µL and vortex 30 s. For the detection of DiD, 100 µL homogenate solutions and 20 µL plasma were mixed with 10 µL 5% glucose and incubated at 37°C for 30 min. Then 8 M urea/methanol (3:2) were added up to 500 µL and vortex 30 s. The final mixed solutions were detected using a fluorescence spectrometer (RF-6000, Shimadzu, Kyoto, Japan). For the detection of BSA-FITC and DiD, the excitation (Ex)/emission (Em) wavelength were 494/524 nm and 644/670 nm, respectively. Standard curves of BSA-FITC and DiD were prepared using blank organ homogenates and plasma, separately.

2.13 Statistical analysis

The results are represented as mean ± standard deviations (S.D.) of at least three independent experiments. Significant differences were identified using Student's *t*-test and one-way ANOVA analysis followed by Bonferroni's post hoc test. A *p*-value of less than 0.05 was statistically significant.

3. Results

3.1 Preparation of RGD-modified nanoparticles

One-step preparation of the nanoparticles encapsulating both the protein and drug is the most attractive aspect in my co-delivery system. In accordance with my former delivery system for drug-drug combination in Chapter I, the ethanol injection method was used in the formulation of this nanoparticle. Multiple components with different charge property and hydrophilicity were involved in this preparation process. The weight ratio of neutral lipid/positive lipid and lipid/protein, the concentration of $CaCO_3$ and the order

of addition were all taken into consideration in the development of nanoparticles. For the optimization, the size, PDI, ζ-potential and drug encapsulation were considered. EPC/protein weight ratio that constituted the skeleton of nanoparticles was first studied. Taking the stability of the nanoparticles and the drug encapsulation of cargos into consideration, the optimal EPC/protein weight ratio was 8:1. EPC/DOTAP weight ratio decided the balance between hydrophobic interactions and electrostatic interactions among lipids and protein that influenced the formation of nanoparticles. At the EPC/DOTAP weight ratio of 10:1, both the nanoparticle characteristics and drug encapsulation were the best. Although high concentration of $CaCO_3$ in the nanoparticles was expected, it affected the stability of nanoparticles. In the preparation, the upmost concentration of encapsulated $CaCO_3$ was 6 mM. After optimization of these factors, the hydrodynamic size and ζ-potential of the nanoparticles were measured (**Table 5**). All the nanoparticle sizes were below 140 nm with enough small PDI (less than 0.3). Insertion of targeting moiety lipid-RGD generated slightly condensed nanoparticles. A charge reversal was observed in both RLBDC/LBDC and RLSPC/LSPC, indicating the successful insertion of RGD peptide-lipids which have net positive charge.

Table 5   Diameter, PDI and ζ potential of nanoparticles

Group	Diameter (nm)	PDI	ζ potential (mV)
LSPC	132.20 ± 0.95	0.179 ± 0.007	-6.78 ± 0.59
RLSPC	129.07 ± 1.48	0.148 ± 0.005	13.53 ± 1.96
LBDC	121.00 ± 0.56	0.276 ± 0.006	-1.65 ± 0.06
RLBDC	111.10 ± 0.36	0.298 ± 0.015	23.37 ± 1.00

Results are expressed as the mean $\pm$ S.D. of three experiments.

The size variation of nanoparticles after mixing with buffer solution of different pH was also detected (**Fig. 15**). LBDC showed an obvious size enlargement from physical condition (pH 7.4) to acidic environment (pH 5.5). PDI and ζ potential slightly changed.

It was suggested that the LBDC might swell as the pH varied, while the integrity of nanoparticles was maintained.

Size Distribution by Intensity

Group	Diameter (nm)	PDI	Zeta potential (mV)
pH 7.4	94.41± 0.43	0.235 ± 0.007	-9.62 ± 0.16
pH 5.5	156.47 ± 2.53	0.230 ± 0.012	-7.06 ± 0.53
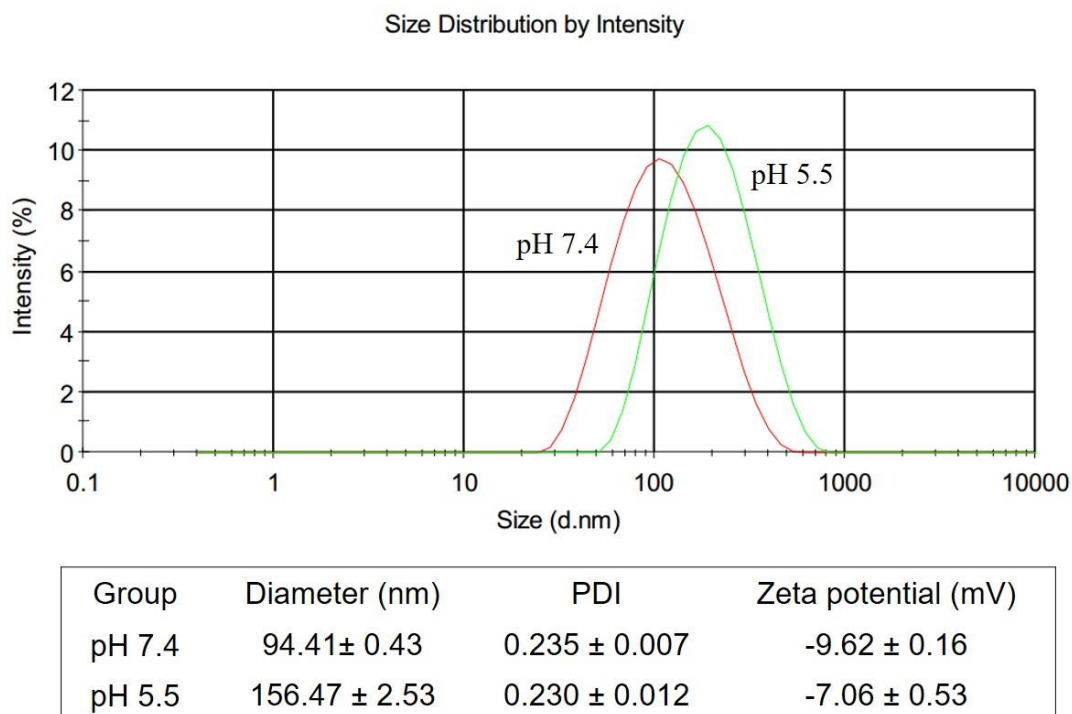
Fig. 15   Particle size, PDI and ζ potential of LBDC in 0.01 M pH 7.4 Hepes buffer and 0.01 M pH 5.5 Mes buffer.

Results are expressed as the mean ± S.D. of three experiments.

3.2 Stability of SOD activity

The enzymatic activity of SOD was tested under various processing conditions and the results showed that SOD maintained normalized activity in a range of 85-110% (**Fig. 16**). It was supposed that the SOD could maintain adequate activity during the preparation of nanoparticles. Note that the activity of SOD at 60°C was not too much decreased even after 2 h. Moreover, after mixing with organic solution for 1 h, which is four times of the process time (15 min), the SOD remained higher than 85% activity in comparison with the control group. Thus, pre-mixing with other components in the ethanol phase for a short period of time did not affect the enzymatic function of SOD in the preparation of nanoparticles.
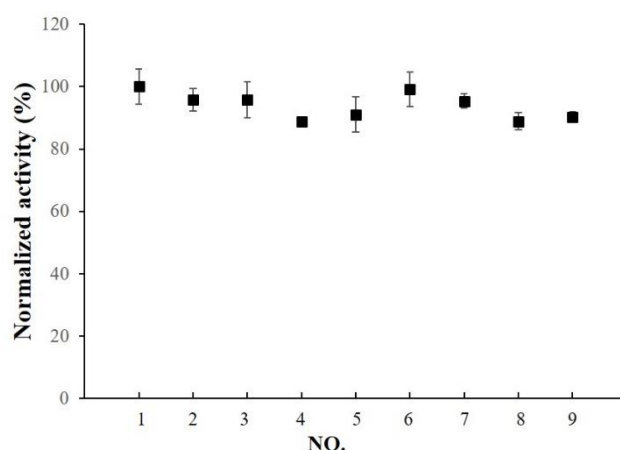
Fig. 16　The normalized activity of SOD after co-incubation.

Each symbol represents the mean ± S.D. of at least three experiments. Experimental conditions (NO.1-9) were indicated in Table 4.

3.3 Encapsulation efficiency of proteins and drugs

Both of BSA-FITC/DiD and SOD/PTX combinations were successfully encapsulated by the carrier. The proteins and drugs showed different encapsulation efficiency in the nanoparticles, while no obvious difference was observed in the encapsulation after lipid-RGD insertion into the nanoparticles (**Fig. 17**). For the small molecules, DiD and PTX have similar content and encapsulation efficiency in the nanoparticles. Although the small molecules, i.e. DiD and PTX showed similar encapsulation efficiency (around 50%), a twice of encapsulation efficiency of BSA (about 60%) was detected with respect to that of SOD (about 30%). It was suggested that the properties of proteins could significantly affected the encapsulation efficiency in these nanoparticles.
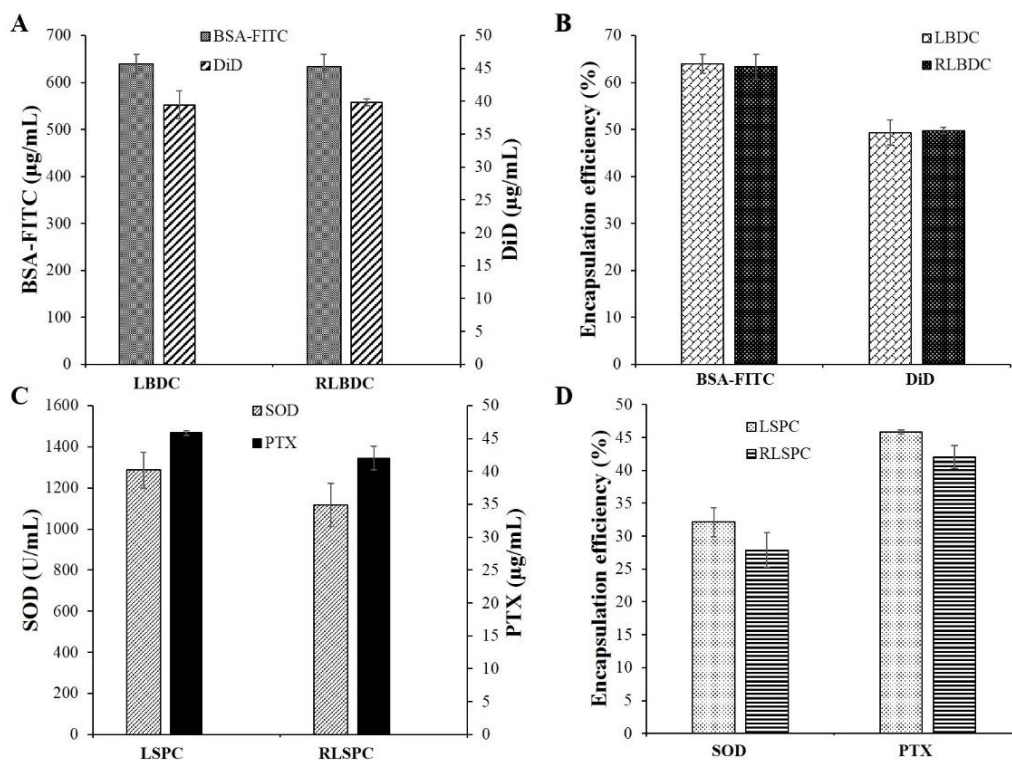
Fig. 17   Encapsulated drug contents and encapsulation efficiencies of both proteins and drugs.
Each bar represents the mean ± S.D. of at least three experiments.

3.4 pH sensitivity in drug release

The release behavior of both BSA-FITC and PTX from RLBPC at different pH was analyzed (**Fig. 18**). BSA-FITC showed a robust pH-sensitive release. A sharply promoted release at initial 1 h reached 40% of total amount in pH 5.5 and around 80% cumulative release at 24 h. A similar and rapid release behavior of PTX was observed in both pH 7.4 and pH 5.5 buffers. Note that almost no PTX release was detected at initial 1 h and then a delayed fast release was detected in both media. It was hypothesized that the insertion position of PTX in the nanoparticles and additive Tween 80 in the media might affect the release rate of PTX. Besides, both BSA-FITC and PTX exhibited a more complete drug release in the end at pH 5.5.
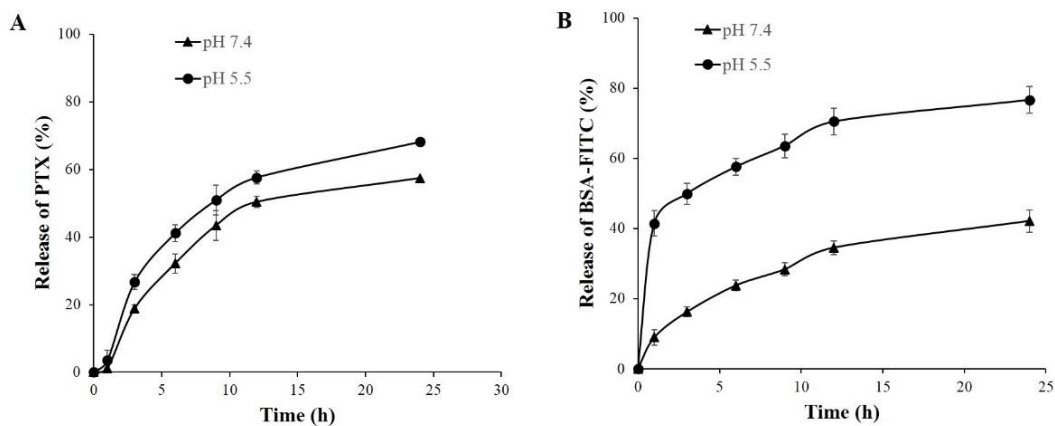
Fig. 18   Drug release of (A) PTX and (B) BSA-FITC from LBPC in 0.01 M pH 7.4 Hepes buffer and 0.01 M pH 5.5 Mes buffer.

For the detection of PTX, 0.1% Tween 80 was included in the release medium. Each symbol represents the mean ± S.D. of at least three experiments.

3.5 Evaluation on the cellular association of nanoparticles

Cellular uptake was studied (**Fig. 19**). BSA-FITC was not detected in the cells after free BSA-FITC and LBDC treatments. However, RGD peptide modification, increased the uptake of BSA-FITC. Because of high lipophilicity of DiD, the membrane association and cellular uptake of free DiD was more impressive than that of RLBDC.
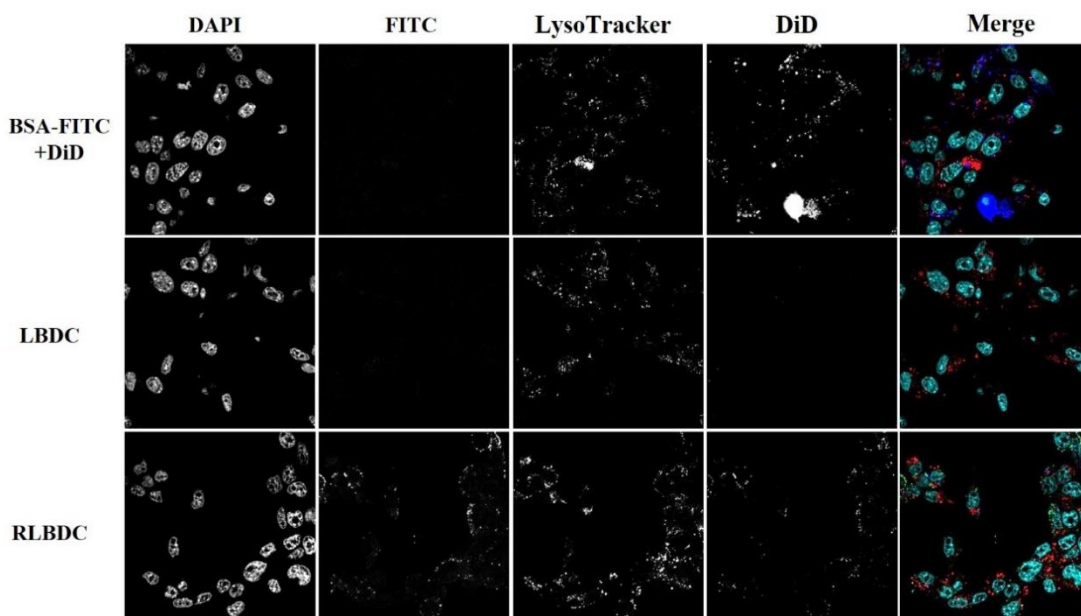
Fig. 19   Cellular association of BSA-FITC + DiD, LBDC and RLBDC 3 h after incubation with the colon 26 tumor cells.

DAPI (nuclei, cyan), BSA-FITC (green), LysoTracker®Red (red) and DiD (blue).

Intracellular localizations of BSA-FITC and DiD in relationship with lysosome/endosome marker were analyzed in an enlarged figure (**Fig. 20**). Entrapped BSA-FITC from RLBDC and intact RLBDC nanoparticles in lysosome/endosome compartments, and escaped RLBDC nanoparticles from lysosome/endosome compartments were partially observed. Importantly, the signals of BSA-FITC and DiD which escaped from lysosome/endosome compartments and released from nanoparticles in the cytosol were observed obviously.
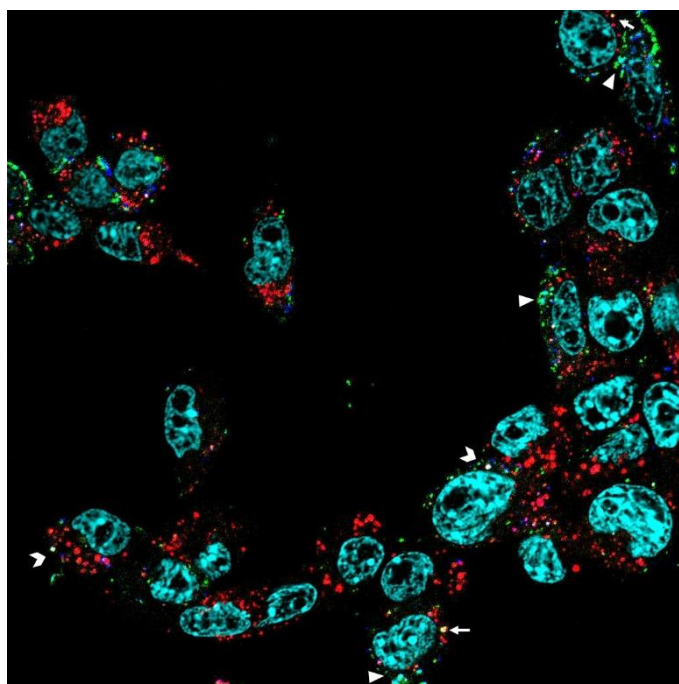
Fig. 20   An enlarged image of cellular uptake of RLBDC at 3 h after incubation.
DAPI (nuclei, cyan), BSA-FITC (green), LysoTracker®Red (red) and DiD (blue). Arrows, V-shaped markers and arrowheads represent entrapped BSA-FITC (the yellow spots, co-localization of green and red) and nanoparticles (white spots, co-localization of green, blue and red) in lysosome/endosome compartments, and escaped nanoparticles from lysosome/endosome compartments (cyan spots, co-localization of green and blue), respectively. Blue and green spots represent released BSA-FITC and DiD in the cytosol, respectively.

The quantitation of RLBDC by a flow cytometer further verified the mechanism of cellular uptake (**Fig. 21**). The mean fluorescence intensity of DiD in RLBDC is 7 times of the group that co-incubated with RLipo, indicating that high concentration of RLipo competitively inhibited the cellular association of RLBDC. It was confirmed that the

increased cellular association of RLBDC was mainly attributed to integrin receptor mediated endocytosis, thereafter the cargos were released into the cytosolic compartment (**Fig. 20**).

Groups	RLBDC	Rlipo + RLBDC
MFI	426 ± 17	57 ± 3
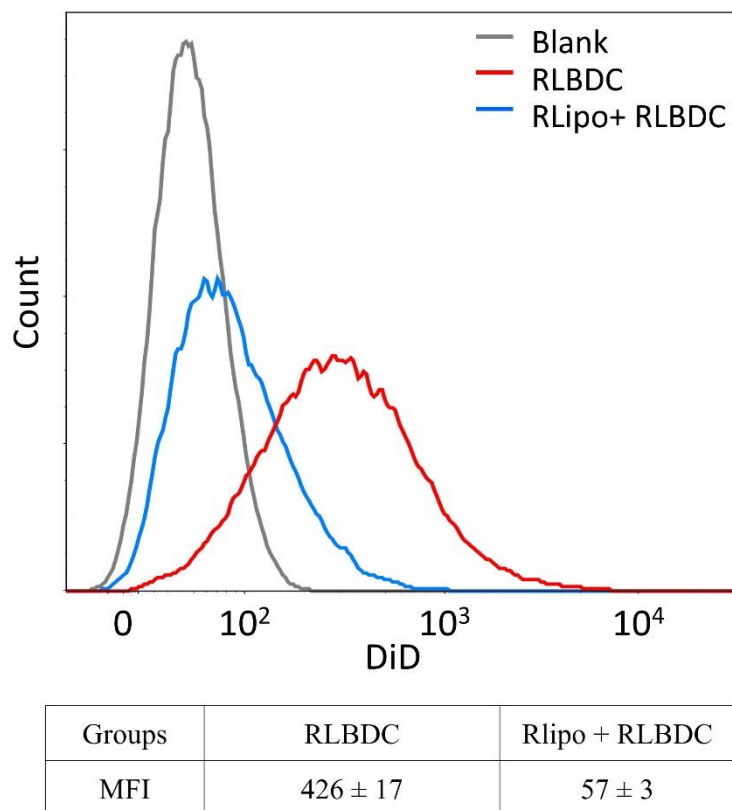
Fig. 21   Quantitation of cellular association of RLBDC and RLipo + RLBDC.
Mean fluorescent intensities (MFIs) are expressed as the mean ± S.D. of three experiments (the MFI of blank cells (50.8) were subtracted).

3.6 Cytotoxicity on the tumor cells

The blank carrier LC and RLC showed no inhibition effect on the colon tumor cells even at the highest concentration of EPC that used in the following study (**Fig. 22**). Cytotoxicity of the nanoparticles was listed in terms of concentration of SOD and PTX (**Fig. 23**). Free SOD showed low cytotoxicity on tumor cells even at the highest concentration, while free PTX possessed stronger cytotoxicity on the colon tumor cells with a concentration dependence. The combination of SOD and PTX solution further improved the inhibition effects on the tumor cells growth. After encapsulation into the nanoparticles, LSPC partly impeded the cytotoxicity of combination therapy on the tumor

cells. Although no significant difference between RLSPC and free SOD + PTX group was observed at the high concentration, RLSPC exhibited the highest cytotoxicity among all preparations, especially in moderate concentrations of SOD (5 U/mL) and PTX (0.2 µg/mL).
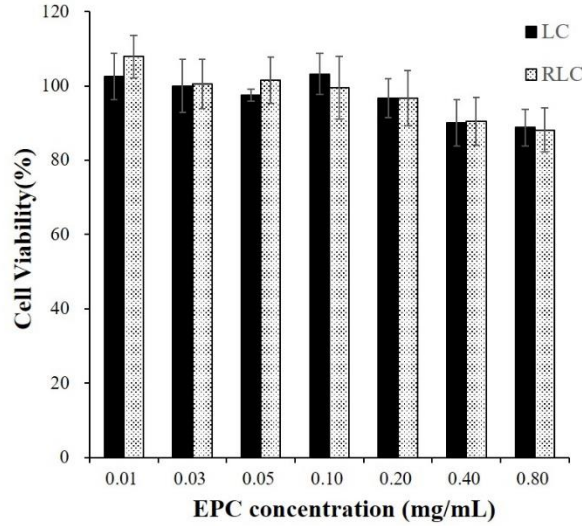
Fig. 22 Cytotoxicity of blank carriers LC and RLC at different concentrations of EPC.
Each bar represents the mean ± S.D. of at least three experiments.
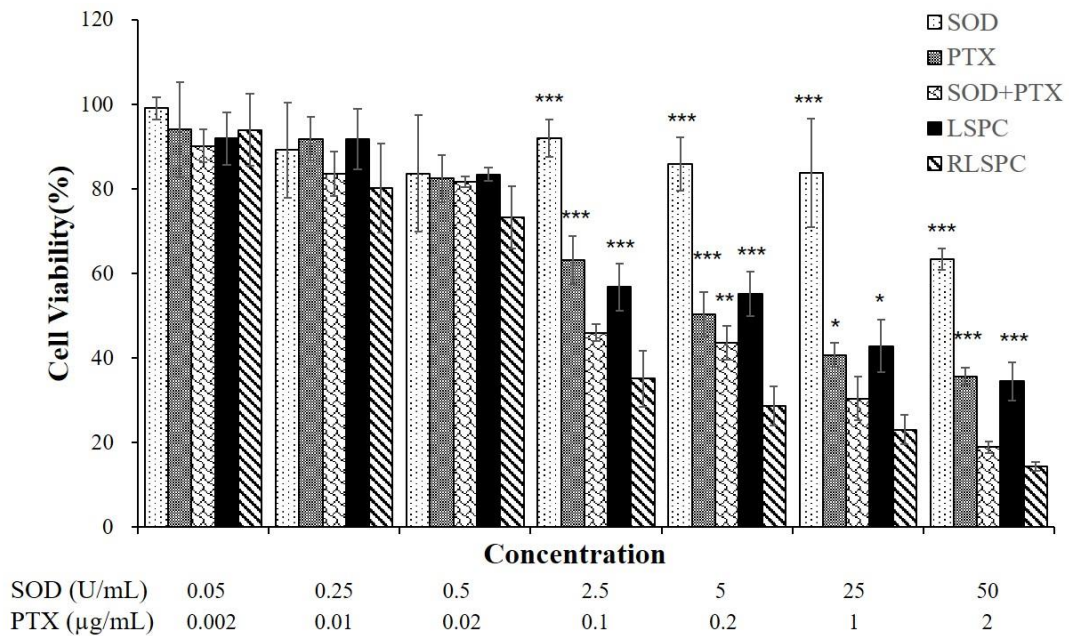
Fig. 23 Cytotoxicity of free SOD, PTX, SOD + PTX, LSPC and RLSPC at the different concentrations of SOD and PTX.
Each bar represents the mean ± S.D. of at least three experiments. Significant differences from RLSPC group were represents as $^*p<0.05$, $^{**}p<0.01$, $^{***}p<0.001$.

3.7 Stability of nanoparticles in FBS solution

Given that the nanoparticles formation was basically based on the electrostatic interactions and hydrophobic interactions between the proteins and lipids, high concentration of serum in circulation might affect the stability of nanoparticles. Evaluation of the protein and drug leakage in the presence of 40% FBS would provide the foundation for the further study *in vivo*. Both of LBDC and RLBDC showed less than 20% leakage of BSA-FITC and DiD (**Fig. 24**). LBDC was more stable compared with RLBDC. RLBDC with positive ζ potential might have more chances for interaction with the serum. Besides, DiD showed a faster leakage from RLBDC in comparison with BSA-FITC, which was in accordance with the release study that drugs (PTX) exhibited faster release at physiological condition (pH 7.4) than proteins (BSA-FITC) (**Fig. 18**).
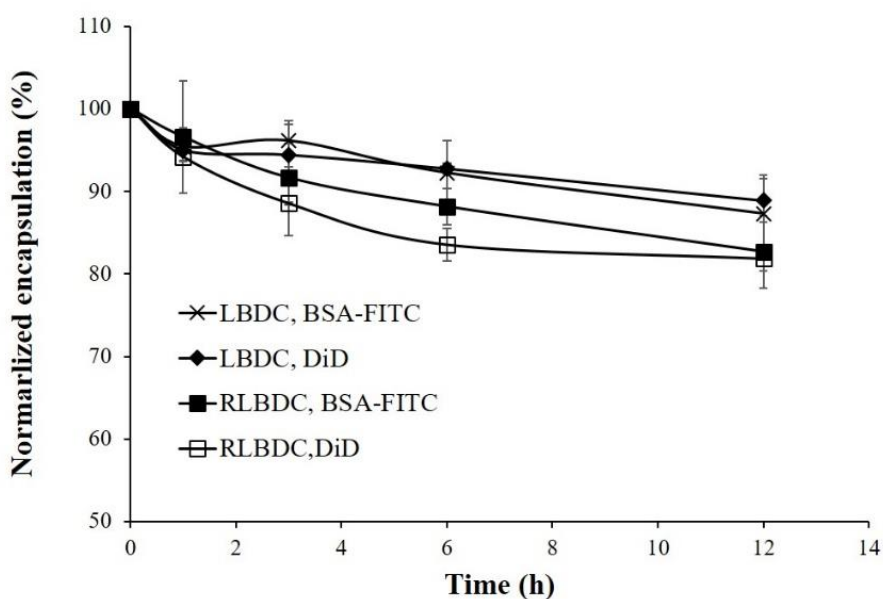
Fig. 24 Stability of LBDC and RLBDC in the presence of 40% (v/v) FBS.
Each symbol represents the mean ± S.D. of at least three experiments.

3.8 Bio-distribution of BSA-FITC and DiD

The aim of bio-distribution experiment was verifying whether the nanoparticles can achieve synchronized distribution of proteins and drugs *in vivo*. Following intravenous administration of free combination solution and LBDC, the plasma concentration of both BSA-FITC and DiD were detected (**Fig. 25**). Plasma concentration of BSA-FITC in

LBDC group was slightly higher than that in free combination at each time point, while the concentration of DiD in LBDC group was 20 times higher than that in free combination group. As a consequence, the LBDC significantly increased the circulation time of DiD *in vivo*. Tissue to plasma (T/P) ratio was used to evaluate the synchronized distribution of BSA-FITC and DiD (**Fig. 26**). The T/P ratios of both BSA-FITC and DiD in LBDC group were under 0.1 for at least 6 h after injection, indicating a good blood circulation property of LBDC. The T/P ratios of BSA-FITC and DiD in LBDC group were comparable in all organs, especially at 1 h (**Fig. 26A**) and 6 h (**Fig. 26B**). About free combination group, the T/P ratio of BSA-FITC and DiD were totally different, especially in the liver, spleen and lung. At 24 h, the accumulation of BSA-FITC and DiD to organs in LBDC group increased differences in T/P ratios between BSA-FITC and DiD (**Fig. 26C**), probably due to the released cargos from nanoparticles. It was indicated that the nanoparticles have successfully achieved synchronized distribution of BSA and DiD *in vivo* for enough long time to expect anticancer efficacy.
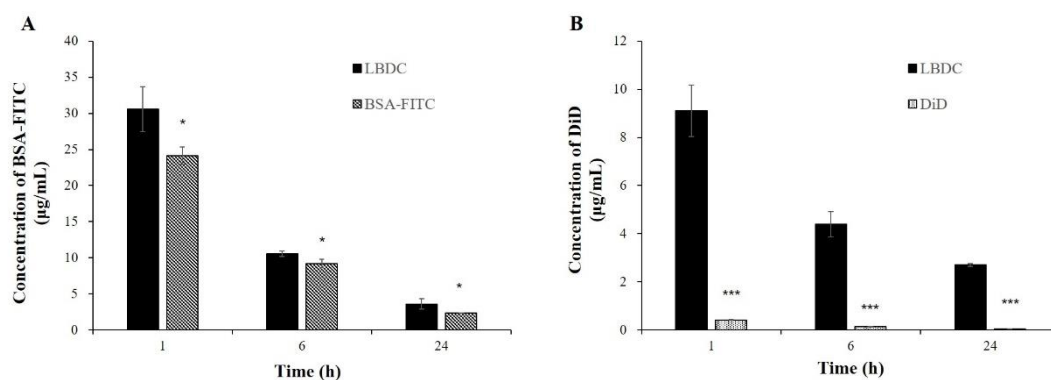
Fig. 25 Plasma concentration of (A) BSA-FITC and (B) DiD from free combination solutions and LBDC in mice at 1, 6 and 24 h after i.v. injection.
Each bar represents the mean ± S.D. of at least three experiments. Significant differences from LBDC group were represents as $^*p<0.05$, $^{***}p<0.001$.
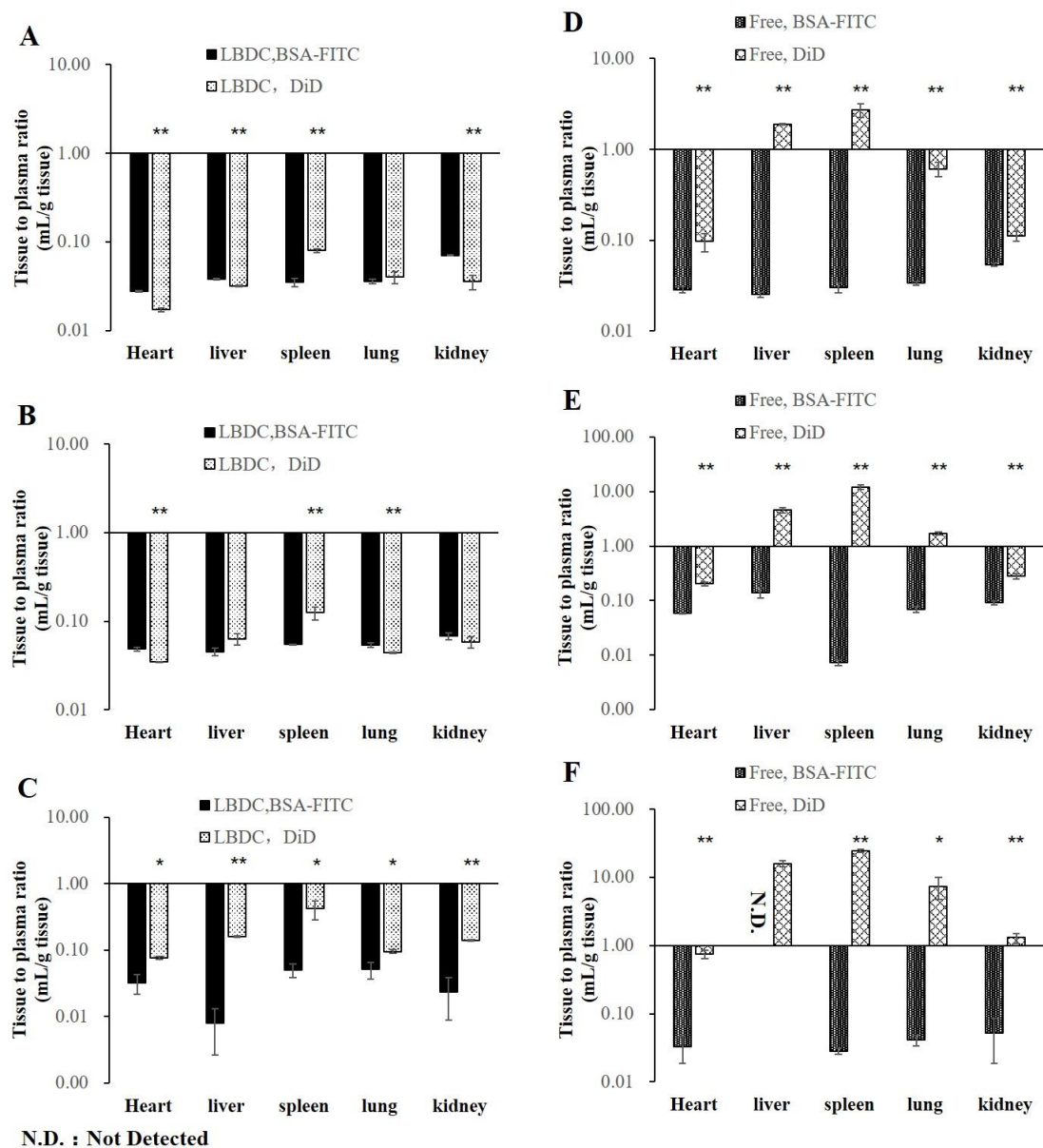
Fig. 26 T/P ratios for BSA-FITC and DiD from (A, B, C) LBDC and (D, E, F) free combination solutions in the heart, liver, spleen, lung and kidney at (A, D) 1, (B, E) 6 and (C, F) 24 h after i.v. injection in mice.

Each bar represents the mean ± S.D. of at least three experiments. Significant differences from BSA-FITC were represents as $^*p<0.01$ and $^{**}p<0.001$. N.D.: not detected.

4. Discussion

The long-term goal of my study is the pursuit of nanoplatforms for co-delivery of the protein and drug combinations that both acting in the cytosol. Such nanoplatforms should involve several characteristics: (1) high encapsulation efficiency of both proteins and

drugs, (2) stimuli-sensitive drug release in cells, (3) stability of nanoparticles in the circulation *in vivo*, (4) synchronized bio-distribution of proteins and drugs, (5) targeting capability to the tumor region. In my previous development of the nanoparticles that encapsulated the doxorubicin and curcumin combination in Chapter I, a polyelectrolyte-polyacrylic acid (PAA) was used to stabilize the nanoparticles containing doxorubicin and $CaCO_3$. Because proteins also belong to a category of polyelectrolytes, I have further developed this drug delivery system to meet the above requirements for the co-delivery of protein/drug combinations.

In this chapter, I have assessed the characteristics of the nanoparticles encapsulating the protein/drug combinations. A BSA-FITC/DiD combination was used for visualization and quantitation of the nanoparticles both *in vitro* and *in vivo*. On the other hand, another SOD/PTX combination was used for cytotoxicity evaluation of the nanoparticles. An ethanol injection method has been implemented in the formulation of nanoparticles to achieve the 'one-step' preparation of the nanoparticles. The choice of ethanol phase and water phase for each component, the order of addition and the specific ratios among the components substantially affected formulation characteristics of the nanoparticles. Thus, it is a big challenge to optimize all these factors mentioned above for successful preparation of the nanoparticles in 'one step' formulation.

During the preparation, PG has played the role of co-solvent for proteins to solubilize in the ethanol phase at a weight ratio of PG: protein = 400:1. It is the key factor in formulating condensed nanoparticles with the 'one-step' preparation. Although the solubility of $CaCl_2$ in ethanol contributed to the successful formation of my former nanoparticles LPCCD [14], the precipitation of proteins in the ethanol phase was observed in the existence of $CaCl_2$. I exchanged the position of $CaCl_2$ and Na_2CO_3 and surprisingly found that the addition of Na_2CO_3 improved the solubility of proteins in the ethanol phase. To guarantee the formation and maintenance of $CaCO_3$ during the removal of alcohols via the ultrafiltration method, a molar ratio of $Ca^{2+}: CO_3^{2-} = 2:1$ was used in the preparation. The order of addition of components in the ethanol phase has determined the

compatibility of components. The interactions between PG and proteins ahead of mixing with EPC prevented the precipitation of proteins induced by promoted intramolecular and intermolecular hydrophobic interactions. After the addition of Na_2CO_3, the pH of ethanol phase above the isoelectric point, promoting the electrostatic interaction between DOTAP and proteins. Meanwhile, the high concentration of EPC added prior to DOTAP interacted with proteins with hydrophobic interactions that restrained the potential co-precipitation formed by DOTAP and proteins induced by electrostatic interactions. In addition, the specific ratios among components affected the properties of the nanoparticles either, especially the ratios among EPC, DOTAP and polyelectrolytes. Unlike the former study that the polymer was in the water phase [14], proteins were added to the ethanol phase in this study, which promoted the interactions of proteins with EPC and DOTAP. Correspondingly, the weight ratio of EPC/DOTAP and polyelectrolyte/DOTAP were decreased from 4:1 to 10:1 and 8:5 to 5:8, respectively. Besides, the capability of proteins possessing low density of carboxyl groups as growth template of $CaCO_3$ was weaker than that of PAA. The concentration of encapsulated $CaCO_3$ decreased to 6 mM in this nanoparticle. The eventual prescription and preparation procedure of the nanoparticles were decided in terms of characteristics of nanoparticles and encapsulation of both proteins and drugs.

The encapsulation efficiency of proteins showed obvious differences (**Fig. 17B and D**). It might be attributed to the different isoelectric points of BSA (PI = 6) and SOD (Cu/Zn Type, PI = 10), molecular weights and methods of quantitation. Because of lower PI of BSA, the electrostatic interactions between DOTAP and BSA-FITC is stronger than SOD enzyme. Single BSA molecule with twice molecular weight possessed stronger interactions with the lipids as an integral than a SOD molecule. Besides, the encapsulated SOD was quantified by the enzymatic activity. Given that part of the SOD activity was lost in the preparation process (**Fig. 16**), it was also partly contributed to the lower encapsulation efficiency of SOD in comparison with BSA-FITC that quantified directly by the fluorescence. It was reasonable to conclude that the physicochemical properties of

proteins would affect the formation of nanoparticles and encapsulation efficiency. A specified regulation on the prescription in accordance with the properties of proteins might be necessary for nanoparticles preparation.

For the evaluation of pH sensitivity, the size variation of nanoparticles and release behavior of cargos were monitored. In the acidic environment, the disruption of $CaCO_3$ might break the balance of electrostatic interactions among the protein/DOTAP/Ca^{2+}/CO_3^{2-}. The nanoparticle size changed with pH variation, indicating the swell of nanoparticles at pH 5.5, while the integrity of the nanoparticles was maintained (**Fig. 15**). It was supposed that the nanoparticles were formed on the basis of electrostatic interactions and hydrophobic interactions. Decreased electrostatic attractions and improved repulsions have partly dissociated the nanoparticles, while the remained hydrophobic interactions have preserved the morphology of nanoparticles to some extent. Moreover, the release behavior of cargos from nanoparticles has further verified the pH sensitivity (**Fig. 18**). The rapid release of BSA-FITC at initial 1 h resulted from the variation of electrostatic interactions. However, decreased release rate of protein after 1 h in both media might attribute to the remained hydrophobic interactions between BSA-FITC and lipids. PTX showed not obvious pH sensitivity in the release. The hydrophobic interaction might be the major factor in the encapsulation of PTX. The fast release of PTX immediately after 1 h indicated the weak interactions between PTX and lipids. It was hypothesized that the interior region of the nanoparticles was occupied by the interactions between BSA-FITC and lipids, subsequently might restrict the deep insertion of PTX. Besides, 0.1% Tween 80 used for the solubilization of PTX might partly promote the release of drug as well. The stimuli-responsive drug release behavior would depend on the interactions between cargos and carriers. A synchronized drug release for cargos might be achieved by coordinating the main interactions of protein/carrier and that of drug/carrier.

High percentage of PEG-lipids was necessary in the formulation of the nanoparticles, while the hydration layer constructed by the PEG on the periphery of the nanoparticles

inhibited the interactions with cells due to steric hindrance [48]. It was the reason that LBDC showed no cellular association during 3 h incubation. RGD peptide has been reported to be employed as the ligand for integrin receptors that overexpressed on the surface of tumor neovasculature endothelial cells and tumor cells [43]. In my study, the inserted RGD peptide on RLBDC could overcome the barrier of PEG layer via SG linker and promoted the cellular uptake of BSA-FITC compared with free combination. Furthermore, the co-localization and separation of the fluorescent signals of BSA-FITC, DiD and lysosomes have demonstrated that the presence of $CaCO_3$ successfully led to endosomal/lysosomal escape and release of cargos to the cytosol (**Fig. 20**). For further verification of integrin receptor-mediated cellular uptake of RLBDC, a RGD peptide modified liposome-RLipo was used for competitive inhibition for integrin receptors. In terms of fluorescence of DiD detected by FACS, the uptake of RLBDC was significantly inhibited by the co-incubation of high concentration of RLipo (**Fig. 21**). It was demonstrated that the promoted cellular uptake of RLBDC was mainly through the integrin receptor-mediated pathway as expected. Although the fluorescence of FITC also decreased in the group of RLipo + RLBDC and a significant difference was detected, the low fluorescence level of FITC in total was unqualified to show the competitive inhibition of cellular uptake (data not shown). Insertion of RGD ligand is a promising strategy to overcome the PEGylation dilemma and improve the cellular uptake of the nanoparticles. Besides, as a flexible unit in the nanoplatform, the targeting ligands can be easily substitute on need.

Correspondingly, the RGD-inserted nanoparticles RLSPC showed the highest inhibition effect on the tumor cell growth *in vitro*, even though free combination of SOD + PTX also exhibited high cytotoxicity, especially at the high concentrations (**Fig. 23**). It was hypothesized that the much longer incubation time in the cytotoxicity study (48 h) enable the interactions and cellular uptake of free drugs eventually. Meanwhile, the improved cytotoxicity of free combination and RLSPC in comparison with the single drugs has verified synergistic effect of the SOD + PTX combination. Although the free

combination exhibited impressive inhibition effects at the high concentrations *in vitro*, RLSPC might be more advantageous to overcome several barriers *in vivo* and realize the inhibition effects at the diseased region.

The *in vivo* distribution of macromolecules and small molecules are totally different [49]. According to the results of bio-distribution study, the circulation time of BSA-FITC in mice was much longer than DiD in the free combination group (**Fig. 25**). However, for the combination therapy, the realization of synergistic effects relies on the efficient co-delivery of combinations to the lesioned organs [50]. Therefore, achieving the synchronized distribution of both proteins and drugs is the main purpose of the DDSs. Initially, the nanoparticles have been verified with sufficient stability in the presence of high concentration of FBS (**Fig. 24**), which is the prerequisite for successful co-delivery. In the bio-distribution study, the similarity in T/P ratios between BSA-FITC and DiD from LBDC in each organ demonstrated that the nanoparticles achieved the synchronized bio-distribution of encapsulated combination, especially before 6 h (**Fig. 26**). In Chapter II, I has provided the foundation for co-delivery of protein/drug combinations at synergistic ratio into tumor region without significant leakage during the circulation in the blood.

5. Conclusion

A novel pH-sensitive nanoplatform for the co-delivery of protein/drug combination was created from the lipids, $CaCO_3$ and cargos (combination of protein/drug). The nanoparticles successfully encapsulated the combinations and kept sufficient stability in the presence of serum. Major destabilization occurred as expected at the acidic environment through the decomposition of $CaCO_3$ that promoted the intracellular drug release. For cellular uptake and cytotoxicity, it was clearly demonstrated that the RGD peptide was the essential part of the nanoparticles for efficient co-delivery of the combinations. PEGylation on the nanoparticles prolonged the circulation of cargos and achieved the synchronized bio-distribution. Here, I proposed a versatile preparation method for targeted protein/drug co-delivery using the nanoplatform with pH sensitivity.

Conclusion

In this thesis, I have developed a 'one-step' preparation method for a novel pH-sensitive nanoplatform for the combination therapies including the small-molecular drugs combinations and the protein/drug combinations. The characteristics of the nanoparticles, *in vitro* cellular uptake and cytotoxicity, *in vivo* stability and bio-distribution have been studied.

1. Key factors in the formulation of nanoparticles

Both nanoparticles developed in Chapter I and Chapter II were formulated based on a nanoplatform consisted of calcium carbonate ($CaCO_3$), lipids, polyelectrolytes and cargos. In comparison with former reported DDSs for combination therapies, 'one-step' preparation of the nanoparticles significantly simplified the preparation procedure and had the potential for wide application. The ethanol injection method, solubility of $CaCl_2$ in ethanol, utilization of co-solvent propylene glycol for solubilization of proteins in the ethanol phase, optimized ratio among components and the order of addition were crucial factors for the successful 'one-step' preparation method.

2. pH sensitivity of nanoparticles

$CaCO_3$ is the stimuli-sensitive unit in the nanoplatform. The concentration of encapsulated $CaCO_3$ was mainly dependent on the interactions between polyelectrolytes and Ca^{2+}. Although the concentration of $CaCO_3$ was different in the nanoparticles, the pH sensitivity of nanoparticles, size variation and drug release behavior were similar. The nanoparticles swelled in the acidic environment but kept the integrity of the particles for a certain period. Both the Dox and protein which were encapsulated basically on the electrostatic interactions showed impressive pH-sensitive release. For the hydrophobic drugs Cur and PTX, no obvious pH-sensitive release was detected due to the remained hydrophobic interactions between drugs and lipids. It was the reason that the pH sensitivity could not destroy the nanoparticles immediately.

3. *In vitro* and *in vivo* evaluation of co-delivery

In cellular uptake studies, the co-localization of fluorescence of the cargos verified successful co-delivery of combination therapies by nanoparticles, which contributed to the improved cytotoxicity of the nanoparticles compared with the free combination solutions. Because of low ratio of PEG insertion, the cellular uptake of Cur and Dox from LPCCD nanoparticles was obvious in the HepG2 cells. However, the high ratio of PEGylation on the periphery of LBDC nanoparticles prevented the cellular uptake. The peptide ligand was necessary for the improvement in cellular uptake and cytotoxicity of the LBDC. *In vivo* studies showed that the nanoparticles for both Cur/Dox and BSA-FITC/DiD combinations prolonged the circulation time and changed the bio-distribution of cargos. For the LBDC with protein/drug combinations, the nanoparticles achieved the synchronized distribution of encapsulated BSA and DiD in mice.

In this study, I have successfully developed the nanoplatform achieving the encapsulation of different combination therapies with simple preparation method. Both *in vitro* and *in vivo* evaluation showed effective co-delivery of cargos from the nanoparticles and enhanced cytotoxicity on the tumor cells.

Acknowledgements

Publications

<u>Peng Jianqing</u>, Fumoto S., Miyamoto, H., Chen, Y., Kuroda, N. & Nishida, K., 2017. One-step formation of lipid-polyacrylic acid-calcium carbonate nanoparticles for co-delivery of doxorubicin and curcumin. *J. Drug Target.*, 25, 704-714.

References

1) Huang W, Wu Q-d, Zhang M, Kong Y-l, Cao P-r, Zheng W, Xu J-h, Ye M: Novel Hsp90 inhibitor FW-04-806 displays potent antitumor effects in HER2-positive breast cancer cells as a single agent or in combination with lapatinib. *Cancer Lett,* **356**, 862-871 (2015).

2) Misra R, Sahoo SK: Coformulation of doxorubicin and curcumin in poly (D, L-lactide-co-glycolide) nanoparticles suppresses the development of multidrug resistance in K562 cells. *Mol Pharm,* **8**, 852-866 (2011).

3) Jiang H, Xu L, Liu D, Liu K, Chen S, Jiang B, Jiang Q, Chen H, Chen Y, Han W: Allogeneic hematopoietic SCT in combination with tyrosine kinase inhibitor treatment compared with TKI treatment alone in CML blast crisis. *Bone Marrow Transplant,* **49**, 1146-1154 (2014).

4) Duan J, Mansour HM, Zhang Y, Deng X, Chen Y, Wang J, Pan Y, Zhao J: Reversion of multidrug resistance by co-encapsulation of doxorubicin and curcumin in chitosan/poly (butyl cyanoacrylate) nanoparticles. *Int J Pharm,* **426**, 193-201 (2012).

5) Pramanik D, Campbell NR, Das S, Gupta S, Chenna V, Bisht S, Sysa-Shah P, Bedja D, Karikari C, Steenbergen C: A composite polymer nanoparticle overcomes multidrug resistance and ameliorates doxorubicin-associated cardiomyopathy. *Oncotarget,* **3**, 640-650 (2012).

6) Wang B-L, Shen Y-m, Zhang Q-w, Li Y-l, Luo M, Liu Z, Li Y, Qian Z-y, Gao X, Shi H-s: Codelivery of curcumin and doxorubicin by MPEG-PCL results in improved efficacy of systemically administered chemotherapy in mice with lung cancer. *Int J Nanomedicine,* **8**, 3521 (2013).

7) Barui S, Saha S, Mondal G, Haseena S, Chaudhuri A: Simultaneous delivery of doxorubicin and curcumin encapsulated in liposomes of pegylated RGDK-lipopeptide to tumor vasculature. *Biomaterials,* **35**, 1643-1656 (2014).

8) Ueno Y, Futagawa H, Takagi Y, Ueno A, Mizushima Y: Drug-incorporating calcium carbonate nanoparticles for a new delivery system. *J Control Release,* **103**, 93-98 (2005).

9) Sharma S, Verma A, Teja BV, Pandey G, Mittapelly N, Trivedi R, Mishra P: An insight into functionalized calcium based inorganic nanomaterials in biomedicine: Trends and transitions. *Colloids Surf B Biointerfaces,* **133**, 120-139 (2015).

10) Zhao D, Wang C-Q, Zhuo R-X, Cheng S-X: Modification of nanostructured calcium carbonate for efficient gene delivery. *Colloids Surf B Biointerfaces,* **118**, 111-116 (2014).

11) Min KH, Min HS, Lee HJ, Park DJ, Yhee JY, Kim K, Kwon IC, Jeong SY, Silvestre OF, Chen X: pH-controlled gas-generating mineralized nanoparticles: a theranostic agent for ultrasound imaging and therapy of cancers. *ACS nano,* **9**, 134-145 (2015).

12) Gong M-Q, Wu J-L, Chen B, Zhuo R-X, Cheng S-X: Self-Assembled

Polymer/Inorganic Hybrid Nanovesicles for Multiple Drug Delivery To Overcome Drug Resistance in Cancer Chemotherapy. *Langmuir,* **31**, 5115-5122 (2015).

13) Kitaeva M, Melik-Nubarov N, Menger F, Yaroslavov A: Doxorubicin-poly (acrylic acid) complexes: interaction with liposomes. *Langmuir,* **20**, 6575-6579 (2004).

14) Peng J, Fumoto S, Miyamoto H, Chen Y, Kuroda N, Nishida K: One-step formation of lipid-polyacrylic acid-calcium carbonate nanoparticles for co-delivery of doxorubicin and curcumin. *J Drug Target,* **25**, 704-714 (2017).

15) Abdalkader R, Kawakami S, Unga J, Suzuki R, Maruyama K, Yamashita F, Hashida M: Evaluation of the potential of doxorubicin loaded microbubbles as a theranostic modality using a murine tumor model. *Acta Biomater,* **19**, 112-118 (2015).

16) Sadzuka Y, Nagamine M, Toyooka T, Ibuki Y, Sonobe T: Beneficial effects of curcumin on antitumor activity and adverse reactions of doxorubicin. *Int J Pharm,* **432**, 42-49 (2012).

17) Li H, Li M, Chen C, Fan A, Kong D, Wang Z, Zhao Y: On-demand combinational delivery of curcumin and doxorubicin via a pH-labile micellar nanocarrier. *Int J Pharm,* **495**, 572-578 (2015).

18) Fang JH, Lai YH, Chiu TL, Chen YY, Hu SH, Chen SY: Magnetic Core–Shell Nanocapsules with Dual-Targeting Capabilities and Co-Delivery of Multiple Drugs to Treat Brain Gliomas. *Adv Healthc Mater,* **3**, 1250-1260 (2014).

19) Li J, Chen Y-C, Tseng Y-C, Mozumdar S, Huang L: Biodegradable calcium phosphate nanoparticle with lipid coating for systemic siRNA delivery. *J Control Release,* **142**, 416-421 (2010).

20) Li J, Yang Y, Huang L: Calcium phosphate nanoparticles with an asymmetric lipid bilayer coating for siRNA delivery to the tumor. *J Control Release,* **158**, 108-114 (2012).

21) Kim SK, Foote MB, Huang L: Targeted delivery of EV peptide to tumor cell cytoplasm using lipid coated calcium carbonate nanoparticles. *Cancer Lett,* **334**, 311-318 (2013).

22) Hu Y, Haynes MT, Wang Y, Liu F, Huang L: A highly efficient synthetic vector: nonhydrodynamic delivery of DNA to hepatocyte nuclei in vivo. *ACS nano,* **7**, 5376-5384 (2013).

23) de Gaetano Donati K, Rabagliati R, Iacoviello L, Cauda R: HIV infection, HAART, and endothelial adhesion molecules: current perspectives. *Lancet Infect Dis,* **4**, 213-222 (2004).

24) Orjuela P, González I, Osorio L: Combination therapy as a strategy to prevent antimalarial drug resistance. *Biomedica,* **24**, 423-437 (2004).

25) Broxterman HJ, Georgopapadakou NH: Anticancer therapeutics:"Addictive" targets, multi-targeted drugs, new drug combinations. *Drug Resist Updat,* **8**, 183-197 (2005).

26) Muggia F: Platinum compounds 30 years after the introduction of cisplatin:

implications for the treatment of ovarian cancer. *Gynecol Oncol,* **112**, 275-281 (2009).

27) Rugo HS: Bevacizumab in the treatment of breast cancer: rationale and current data. *Oncologist,* **9**, 43-49 (2004).

28) Miao L, Guo S, Lin CM, Liu Q, Huang L: Nanoformulations for Combination or Cascade Anticancer Therapy. *Adv Drug Deliv Rev*, (2017).

29) Leader B, Baca QJ, Golan DE: Protein therapeutics: a summary and pharmacological classification. *Nat Rev Drug Discov,* **7**, 21-39 (2008).

30) Yu M, Wu J, Shi J, Farokhzad OC: Nanotechnology for protein delivery: Overview and perspectives. *J Control Release,* **240**, 24-37 (2016).

31) Jiang T, Sun W, Zhu Q, Burns NA, Khan SA, Mo R, Gu Z: Furin-Mediated Sequential Delivery of Anticancer Cytokine and Small-Molecule Drug Shuttled by Graphene. *Adv Mater,* **27**, 1021-1028 (2015).

32) Monterrubio C, Paco S, Olaciregui NG, Pascual-Pasto G, Vila-Ubach M, Cuadrado-Vilanova M, Ferrandiz MM, Castillo-Ecija H, Glisoni R, Kuplennik N: Targeted drug distribution in tumor extracellular fluid of GD2-expressing neuroblastoma patient-derived xenografts using SN-38-loaded nanoparticles conjugated to the monoclonal antibody 3F8. *J Control Release,* **255**, 108-119 (2017).

33) Shein SA, Kuznetsov II, Abakumova TO, Chelushkin PS, Melnikov PA, Korchagina AA, Bychkov DA, Seregina IF, Bolshov MA, Kabanov AV: VEGF- and VEGFR2-Targeted Liposomes for Cisplatin Delivery to Glioma Cells. *Mol Pharm,* **13**, 3712-3723 (2016).

34) Jin J-l, Gong J, Yin T-j, Lu Y-j, Xia J-j, Xie Y-y, Di Y, He L, Guo J-l, Sun J: PTD4-apoptin protein and dacarbazine show a synergistic antitumor effect on B16-F1 melanoma in vitro and in vivo. *Eur J Pharmacol,* **654**, 17-25 (2011).

35) Olijslagers SJ, Zhang YH, Backendorf C, Noteborn MH: Additive cytotoxic effect of apoptin and chemotherapeutic agents paclitaxel and etoposide on human tumour cells. *Basic Clin Pharmacol Toxicol,* **100**, 127-131 (2007).

36) Song Y, Xin X, Zhai X, Xia Z, Shen K: Sequential combination therapy with flavopiridol and autocatalytic caspase-3 driven by amplified hTERT promoter synergistically suppresses human ovarian carcinoma growth in vitro and in mice. *J Ovarian Res,* **7**, 121 (2014).

37) Schieber M, Chandel NS: ROS function in redox signaling and oxidative stress. *Curr Biol,* **24**, R453-R462 (2014).

38) Cairns RA, Harris IS, Mak TW: Regulation of cancer cell metabolism. *Nat Rev Cancer,* **11**, 85-95 (2011).

39) Benhar M, Dalyot I, Engelberg D, Levitzki A: Enhanced ROS production in oncogenically transformed cells potentiates c-Jun N-terminal kinase and p38 mitogen-activated protein kinase activation and sensitization to genotoxic stress. *Mol Cell Biol,* **21**, 6913-6926 (2001).

40) Laurent A, Nicco C, Chéreau C, Goulvestre C, Alexandre J, Alves A, Lévy E, Goldwasser F, Panis Y, Soubrane O: Controlling tumor growth by modulating

endogenous production of reactive oxygen species. *Cancer Res,* **65**, 948-956 (2005).

41) Wang M, Alberti K, Sun S, Arellano CL, Xu Q: Combinatorially Designed Lipid-like Nanoparticles for Intracellular Delivery of Cytotoxic Protein for Cancer Therapy. *Angew Chem Int Ed Engl,* **126**, 2937-2942 (2014).

42) Amin M, Mansourian M, Koning G, Badiee A, Jaafari M, Ten Hagen T: Development of a novel cyclic RGD peptide for multiple targeting approaches of liposomes to tumor region. *J Control Release,* **220**, 308-315 (2015).

43) Desgrosellier J, Cheresh D: Integrins in cancer: biological implications and therapeutic opportunities. *Nat. Rev. Cancer,* **10**, 9-22 (2010).

44) Suga T, Fuchigami Y, Hagimori M, Kawakami S: Ligand peptide-grafted PEGylated liposomes using HER2 targeted peptide-lipid derivatives for targeted delivery in breast cancer cells: The effect of serine-glycine repeated peptides as a spacer. *Int J Pharm,* **521**, 361-364 (2017).

45) Suga T, Kawakami S: unpublished work.

46) Harlow E, Lane D: A laboratory manual. *Cold Spring Harbor Laboratory,* **579**, (1988).

47) Ke M, Fujimoto S, Imai T: SeeDB: a simple and morphology-preserving optical clearing agent for neuronal circuit reconstruction. *Nat. Neurosci.,* **16**, 1154-1161 (2013).

48) Hama S, Itakura S, Nakai M, Nakayama K, Morimoto S, Suzuki S, Kogure K: Overcoming the polyethylene glycol dilemma via pathological environment-sensitive change of the surface property of nanoparticles for cellular entry. *J Control Release,* **206**, 67-74 (2015).

49) Vasquez K, Casavant C, Peterson J: Quantitative whole body biodistribution of fluorescent-labeled agents by non-invasive tomographic imaging. *PLoS ONE,* **6**, e20594 (2011).

50) Guo S, Lin C, Xu Z, Miao L, Wang Y, Huang L: Co-delivery of cisplatin and rapamycin for enhanced anticancer therapy through synergistic effects and microenvironment modulation. *ACS Nano,* **8**, 4996-5009 (2014).